MOUNTAIN-PLAINS CONSORTIUM

MPC 19-390 | S. Chen and Y. Zhou

Interaction Analysis of Long-span Bridges and Traffic System Subjected to Earthquakes

MOUNTAIN-PLAINS CONSORTIUM REGION 8

A University Transportation Center sponsored by the U.S. Department of Transportation serving the Mountain-Plains Region. Consortium members:

Colorado State University
North Dakota State University
South Dakota State University
University of Colorado Denver
University of Denver
University of Utah
Utah State University
University of Wyoming

Interaction Analysis of Long-span Bridges and Traffic System Subjected to Earthquakes

Suren Chen
Yufen Zhou

Department of Civil and Environmental Engineering
Colorado State University
Fort Collins, CO 80523

July 2019

Acknowledgements

The funds for this study were provided by the United States Department of Transportation to the Mountain-Plains Consortium (MPC).

Disclaimer

The contents of this report reflect the views of the authors, who are responsible for the facts and the accuracy of the information presented. This document is disseminated under the sponsorship of the Department of Transportation, University Transportation Centers Program, in the interest of information exchange. The U.S. Government assumes no liability for the contents or use thereof.

ABSTRACT[1]

Long-span bridges support a large amount of traffic every day. Even when an earthquake strikes, a long-span bridge often still has many vehicles present due to the low predictability of earthquake events. To study the seismic performance of bridge and traffic systems, a new full-response prediction methodology for the coupled bridge-traffic interaction system under spatially varying earthquake excitations was developed by capturing the interaction effects not only between the bridge and moving vehicles, but also between earthquake excitations and the coupled bridge-traffic system. Different from existing bridge seismic analyses in which only traditional earthquake loads in terms of inertial forces are applied on the bridge structure, the new formulation can also incorporate coupled earthquake forces on the bridge and vehicles, which are expressed as functions of the bridge-traffic coupling matrices and earthquake displacement inputs. The proposed methodology was numerically demonstrated on a prototype long-span bridge and traffic system under spatially varying earthquake excitations. Responses of the bridge and vehicles were predicted when the bridge-traffic system was subjected to earthquake excitations. It was determined from the numerical analysis that the coupled earthquake force, as derived in this study, has notable influence on the dynamic performance of the bridge and vehicles under seismic excitations.

[1] This study has been published as a journal paper: Zhou, Y. and Chen, S. (2018). "Full-response prediction of the coupled long-span bridge and traffic system under spatially varying seismic excitations", *Journal of Bridge Engineering, ASCE*, 23(6): 04018031.

TABLE OF CONTENTS

LIST OF TABLES

LIST OF FIGURES

EXECUTIVE SUMMARY

Many long-span bridges have been built around the world to cross major rivers and straits. Despite the high flexibility and low inherent damping, long-span bridges are vulnerable to possible damage and reduction of functionality following earthquake events. Long-span bridges support a significant amount of traffic every day, and many vehicles are likely present when an earthquake strikes the bridge site due to poor predictability of earthquake events. Traditional bridge seismic studies typically dealt with seismic loads acting on a bridge structure without appropriately considering the traffic as dynamic loads. The extensive damages observed on existing bridges and significance of maximizing functionality of future long-span bridges following earthquakes highlight the continuing research needs on understanding the seismic performance and further improving the resilience of long-span bridges against earthquakes.

This study develops a full-response interaction assessment framework that predicts the seismic performance of the coupled bridge-traffic system by appropriately modeling the coupling effects between the spatially varying earthquake loads and bridge-traffic system. First, formulation of the full-response analytical framework of the bridge-traffic system subjected to earthquakes is derived starting from the motion equations on the bridge constrained and unconstrained degrees of freedom. The coupling effects among the bridge structure, individual vehicles and earthquake excitations are comprehensively incorporated. The developed framework is further demonstrated on a prototype long-span bridge-traffic system under spatially varying seismic excitations. Full responses for the bridge and moving vehicles are evaluated and the effect of moving traffic on the bridge seismic performance is investigated with the proposed assessment framework. Finally, the coupling forces between earthquakes and the bridge-traffic system are quantified and their influences on the seismic performance of the bridge and moving vehicles are discussed.

1. INTRODUCTION AND LITERATURE REVIEW

1.1 BACKGROUND

Many long-span bridges have been built around the world to cross major rivers and straits. Despite the high flexibility and low inherent damping, long-span bridges are vulnerable to possible damage and reduction of functionality following earthquake events.

Different from short-span and medium-span bridges, long-span bridges rarely experience total collapse when subjected to earthquakes. However, severe damage, extensive repair and associated traffic disruptions following a major earthquake can become a disaster for regional transportation and economy, given the fact that these bridges usually connect major corridors as lifeline infrastructures. Recent examples include Chi-Lu Bridge during the 1999 Taiwan Chi-Chi earthquake, San Francisco–Oakland Bay Bridge following 1989 Loma Prieta earthquake and Higashi-Kobe Bridge due to 1995 Kobe earthquake. As a type of critical civil infrastructures, long-span bridges often play a crucial role in emergency response, evacuation of affected people and restoration of post-hazard functionality of the transportation network.

The extensive damages observed on existing bridges and significance of maximizing functionality of future long-span bridges following earthquakes highlight the continuing research needs on understanding the seismic performance and further improving the resilience of long-span bridges against earthquakes.

1.2 LITERATURE REVIEW

1.2.1 Seismic Analysis of Bridge-traffic System

Long-span bridges support a significant amount of traffic every day, and many vehicles are likely present when an earthquake strikes the bridge site due to poor predictability of earthquake events. Traditional bridge seismic studies typically dealt with seismic loads acting on a bridge structure without appropriately considering the traffic as dynamic loads.

Liu et al. (2011) studied the dynamic effect of a simple suspension bridge model regarding moving vehicle loads. In the study, vehicles were simplified as moving loads; therefore, the bridge and vehicles were not physically coupled in a system and vibrating effects from vehicles could not be incorporated. Li et al. (2012) investigated the effects of seismic excitations on the coupled vehicle-bridge system by assuming that a number of equally distributed vehicles move through the bridge at a constant speed.

A study by Du et al. (2012) looked into the seismic performance of a long-span bridge and considered interaction effects from the moving train using seismic displacement loading approach. A recent study by Zeng and Dimitrakopoulos (2016) established a scheme for the seismic analysis of interacting train–bridge systems considering the coupling effects between the bridge, train and uniform earthquake excitations. It is known that the vehicles in the highway traffic flow move in a stochastic nature and may experience acceleration, deceleration and braking, and the adoption of a deterministic series of vehicles may not realistically represent the traffic on a bridge when an earthquake occurs.

1.2.2 Bridge-traffic Dynamic Interaction Analysis

In a recent study by Zhou and Chen (2015a), stochastic traffic flow was simulated to consider the vehicle acceleration, deceleration, braking and lane changing behaviors by following certain traffic rules. The bridge and each individual vehicle were directly coupled under seismic excitations at the bridge supports. As a result, more reasonable estimation of the dynamic response of the bridge-traffic system under seismic excitations can be made by appropriately modeling the dynamic interaction of the bridge-traffic system.

For long-span bridges, spatial variability effects of seismic excitations are critical and were also considered in the study by Zhou and Chen (2015a). However, in nearly all existing studies related to vehicles and highway bridges, the earthquake loads were still derived from the bridge structure directly without considering coupling effects between the spatially varying earthquake excitations and interacting bridge-traffic system. Consequentially, the influence of the coupling effects between the spatially varying seismic excitations and bridge-traffic system has hardly been incorporated into the seismic response prediction of the bridge and moving vehicles.

Wind hazard is another type of major hazard critical to long-span bridges. It has been extensively studied in terms of coupling effects between the wind loads and bridge-traffic system. It was found that such coupling effects can be rather significant (e.g., Chen and Wu 2010; Zhou and Chen 2015a, b). In contrast, the coupling effect between the spatially-varying earthquake loads and highway bridge-traffic system has never been modeled and studied in literatures, and it remains unclear what the nature and significance of such coupling effects on the dynamic response of the long-span bridge-traffic system.

1.3 ORGANIZATION OF THIS REPORT

This study aims to develop a full-response assessment framework that predicts the seismic performance of the coupled bridge-traffic system by appropriately modeling the coupling effects between the spatially varying earthquake loads and bridge-traffic system.

First, formulation of the full-response analytical framework of the bridge-traffic system subjected to earthquakes is derived starting from the motion equations on the bridge constrained and unconstrained degrees of freedom. The coupling effects among the bridge structure, individual vehicles and earthquake excitations are comprehensively incorporated.

The developed framework is then demonstrated on a prototype long-span bridge-traffic system under spatially varying seismic excitations. Full responses for the bridge and moving vehicles are evaluated and the effect of moving traffic on the bridge seismic performance is investigated with the proposed assessment framework.

Finally, the coupling forces between earthquakes and the bridge-traffic system are quantified and their influences on the seismic performance of the bridge and moving vehicles are discussed.

The report is composed of five sections. Section 1 introduces pertinent background information and literature review results related to the present study. In Section 2, the modeling process of bridge and traffic flow is introduced. In Section 3, the methodology of coupled seismic analysis and bridge system is introduced. In Section 4, numerical analysis of the bridge traffic-system subjected to earthquakes is conducted and results are discussed. The report concludes with Section 5.

2. DYNAMIC MODELING OF BRIDGE AND TRAFFIC

It is known that the formulation of a bridge-vehicle interaction model is dependent on instantaneous response of the bridge and each individual vehicle. Therefore, the dynamic analysis must proceed iteratively at each time step, which presents a challenge for common commercial finite element programs, since it is difficult for built-in modules of most software to incorporate iterative analysis functions. However, commercial finite element programs have advantages in sophisticated finite element formulations, nonlinear effect considerations and advanced meshing options, which make them good candidates for detailed modeling of bridge deck of a multi-span highway bridge.

The hybrid bridge dynamic model combines the finite element bridge model and the mode-based bridge-traffic interaction model. In the mode-based bridge-traffic interaction model, the bridge is modeled using modal coordinates and vehicles are modeled using physical coordinates. The bridge displacement response can be obtained through analysis as the primary bridge responses. The dynamic displacement response of each individual vehicle can also be obtained from the simulation analysis. By adopting plate-bending theory, the detailed bridge deck response including strain, stress and internal forces can be obtained through applying the finite element shape functions.

2.1 Modeling of the Bridge

The bridge structure is built as a three-dimensional finite element model in the commercial finite element program SAP2000. Each node on the bridge structure has six degrees of freedom (DOFs), which include three translational DOFs in the x, y and z directions and three rotational DOFs around x, y and z directions. The nonlinear static analysis under gravity forces and initial cable stress is conducted on the bridge structure to determine the equilibrium position as the initial deformed state. Eigenvalue analysis is conducted based on the mass and stiffness matrices of the deformed bridge structure from the nonlinear static analysis. This is done to obtain modal properties for all the modes, including frequencies and mode shapes. Following the multi-mode superposition approach, a number of modes of the bridge are selected to develop bridge motion equations, as shown in the next section, for the following bridge-traffic interaction analysis under earthquake excitations.

2.2 Dynamic Modeling of Traffic Flow

2.2.1 Vehicle Dynamic Model

To replicate realistic traffic situation on long-span bridges, the bridge-traffic system was established and based on the bridge structure and all vehicles in the stochastic traffic flow. The stochastic traffic flow in this study is simulated using the cellular automaton (CA) traffic simulation model. The CA-based traffic flow simulation is conducted on a “roadway-bridge-roadway” route to replicate the stochastic traffic flow through the bridge following the approach proposed by Chen and Wu (2011). vehicles move through the roadway-bridge-roadway path following probabilistic traffic rules, which regulate the acceleration, deceleration, lane changing and braking maneuvers.

Vehicles in the stochastic traffic are categorized into three types from several vehicle configurations: heavy truck with one trailer, light truck, and light car (Chen and Wu 2010). The vehicles are modeled as a combination of several rigid bodies and wheel axles connected with series of springs and dampers in vertical and lateral directions. The displacement vector $\mathbf{d}_{vh}$ for the heavy truck model contains 19 DOFs including eight independent vertical, eight lateral and three rotational DOFs respectively, which is defined in Eq. (1). The dimensional parameters and DOFs of the heavy truck model are shown in Figure 2.1a and 2.1b.

$$\mathbf{d}_{\mathbf{vh}} = \{Z_{r1}\ \theta_{r1}\ \beta_{r1}\ Z_{r2}\ \beta_{r2}\ Z_{a1L}\ Z_{a1R}\ Z_{a2L}\ Z_{a2R}\ Z_{a3L}\ Z_{a3R}\ Y_{r1}\ Y_{r2}\ Y_{a1L}\ Y_{a1R}\ Y_{a2L}\ Y_{a2R}\ Y_{a3L}\ Y_{a3R}\} \quad \text{(Eq. 1)}$$

in which, Z, Y, θ, and β are the vertical, lateral, pitching and rolling displacements, respectively. The subscripts r, a, $L(R)$ denote rigid body, wheel axle, left (right) side, respectively. The subscripts 1, 2, and 3 represent the rigid body number or wheel axle number.

The displacement vector $\mathbf{d}_{\mathbf{vl}}$ for the light truck and light car has 12 DOFs including five independent vertical, five lateral and two rotational DOFs, respectively, as demonstrated in Eq. (2). The dimensional parameters and DOFs of the light truck and light car models are shown in Figure 2.2 in elevation view and Figure 2.1b in front view.

$$\mathbf{d}_{\mathbf{vl}} = \{Z_{r1}\ \theta_{r1}\ \beta_{r1}\ Z_{a1L}\ Z_{a1R}\ Z_{a2L}\ Z_{a2R}\ Y_{r1}\ Y_{a1L}\ Y_{a1R}\ Y_{a2L}\ Y_{a2R}\} \quad \text{(Eq. 2)}$$

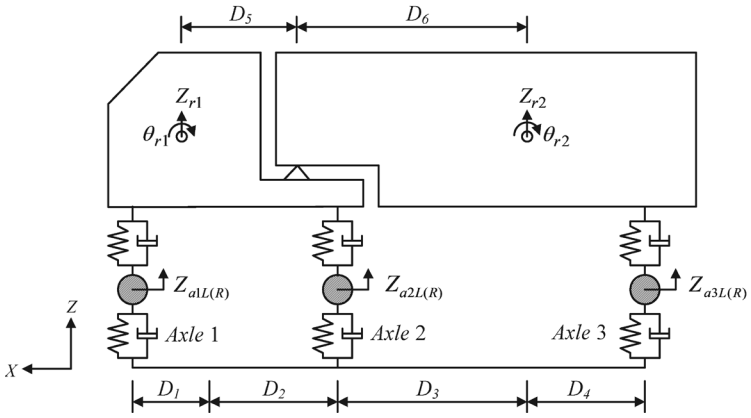

(a) Elevation view

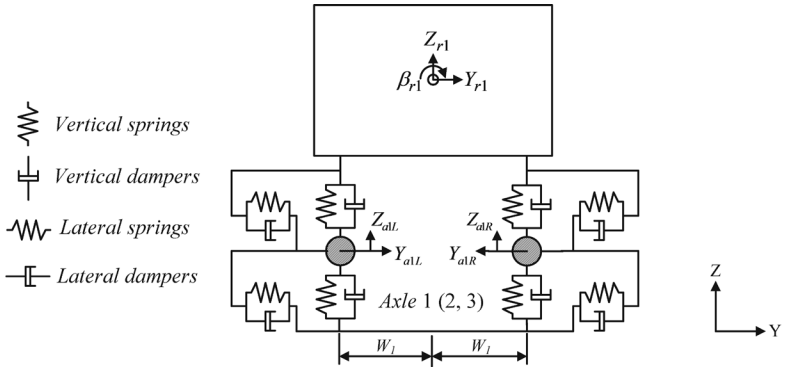

(b) Front view

Figure 2.1 Elevation view and front view for the numerical model of heavy truck

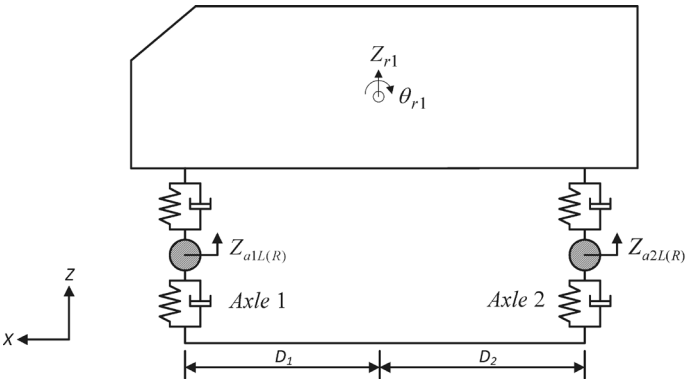

Figure 2.2 Elevation view for the numerical model of the light truck and light car

2.2.2 Stochastic Traffic Flow Simulation

In this study, the three-lane cellular automaton model is adopted to simulate the instantaneous behavior of vehicles temporally and spatially. As a mathematical idealization of physical systems with discrete time and space, cellular automaton consists of a finite set of discrete variables to represent specific vehicle information. The discrete variables for any individual vehicle include its occupied lane, longitudinal location, type, speed, and driving direction. Variables in each cellular are updated based on the adjacent vehicle information and the probabilistic traffic rules regulating accelerating, decelerating, lane changing and braking. Detailed traffic rules involved in the traffic flow simulation are referred to in the published paper (Chen and Wu 2010). The cellular automaton-based traffic flow simulation is performed on a roadway-bridge-roadway system to simulate the stochastic traffic flow through the bridge in a realistic way.

Randomization of the traffic flow is realized by stochastic initial variables in the cellular of the whole system. Periodic boundary conditions are adopted in the traffic flow model, in which the total number of each type of vehicles in the system remains constant. Vehicles in the simulated traffic flow are classified into three types: heavy multi-axle truck, light truck, and sedan. Vehicle classification ratios that define the composition of different types of vehicles in the traffic flow are usually quantified based on the site-specific traffic data or generic traffic statistics when the specific data is not available.

3. METHDOLOGY ON COUPLED SEISMIC ANALYSIS OF BRIDGE/TRAFFIC SYSTEM

3.1 Simulation of Spatially Varying Earthquake Ground Motion

3.1.1 Generation of Power Spectrum Density Function (PSDF)

Earthquake ground motion records are typical nonstationary random processes; therefore, it is important to incorporate the non-stationary properties in the simulation of earthquake ground motions. In this study, nonstationary properties of simulated earthquake ground motions are assumed to be similar to a scenario earthquake record in terms of the evolutionary power spectrum density function (PSDF). The evolutionary PSDF of the scenario earthquake is obtained by means of the Short-Time Fourier Transform (STFT) or the Wavelet Transform (WT) from which the time-varying frequency distribution of the nonstationary processes with a chosen window or wavelet is represented.

3.1.2 Simulation of Earthquake Ground Motions Considering Spatial Variability

With the spectral representation method, the spatially varying earthquake ground motion at each support is simulated as one-dimensional, n-variate non-stationary Gaussian random process with certain evolutionary PSDF. The cross spectral density matrix for the one-dimensional, n-variate non-stationary stochastic process with components $f_1(t)$, $f_2(t)$, …, $f_n(t)$ can be expressed in the following equation.

$$\mathbf{S}(\omega,t)=\begin{bmatrix} S_{11}(\omega,t) & S_{12}(\omega,t) & \cdots & S_{1n}(\omega,t) \\ S_{21}(\omega,t) & S_{22}(\omega,t) & \cdots & S_{2n}(\omega,t) \\ \vdots & \vdots & \ddots & \vdots \\ S_{n1}(\omega,t) & S_{n2}(\omega,t) & \cdots & S_{nn}(\omega,t) \end{bmatrix} \quad \text{(Eq. 3)}$$

in which, $S_{ii}(\omega,t)$ is the evolutionary power spectral density function of the i^{th} component $f_i(t)$; $S_{ij}(\omega,t)$ is the cross power spectral density function between the i^{th} component and the j^{th} component; $S_{ij}(\omega,t)=\Gamma_{ij}\sqrt{S_i(\omega)S_j(\omega)}$; Γ_{ij} is the complex coherence function between the i^{th} component and the j^{th} component.

The cross density matrix is decomposed using the Cholesky's method at every frequency and time instant into this form:

$$\mathbf{S}(\omega,t)=\mathbf{H}(\omega,t)\mathbf{H}^{\mathbf{T}*}(\omega,t) \quad \text{(Eq. 4)}$$

in which, $\mathbf{H}(\omega,t)$ is the lower triangle matrix from the Cholesky decomposition of $\mathbf{S}(\omega,t)$; $\mathbf{H}^{\mathbf{T}*}(\omega,t)$ is the transpose form of the complex conjugate matrix for $\mathbf{H}(\omega,t)$.

After decomposition of the cross spectral matrix, the non-stationary stochastic process for components $f_1(t)$, $f_2(t)$, …, $f_n(t)$ can be simulated with the following equation (Deodatis 1996):

$$f_i(t)=\frac{2}{\sqrt{2\pi}}\sum_{m}^{i}\sum_{l=1}^{N}\left|H_{im}(\omega_l,t)\right|\sqrt{\Delta\omega}\cos[\omega_l t-\theta_{im}(\omega_l,t)+\Phi_{ml}] \quad \text{(Eq. 5)}$$

in which, N is the number of division of the frequency range; $\omega_l = l\Delta\omega$, l = 1, 2, …, N; $\Delta\omega = \omega_u / N$; ω_u represents an upper cut-off frequency; Φ_{ml} is the independent random phase angle, which is distributed uniformly in the range of 0 to 2π; $\theta_{im}(\omega_l, t) = \tan^{-1}(\mathrm{Im}(H_{im}(\omega_l, t))/\mathrm{Re}(H_{im}(\omega_l, t)))$.

3.1.3 Generation of Earthquake Ground Motion Velocity and Displacement Histories

During the simulation process of spatially varying earthquake ground motions, very high or very low frequency contents may be associated with simulated acceleration time histories. Therefore, a Butterworth filter with a bandpass frequency region is applied on the simulated acceleration histories to eliminate very high or low frequency contents. Through the simulated earthquake acceleration histories, the earthquake velocity and displacement histories can be obtained through single numerical integration and double numerical integration with respect to time, respectively. The numerical integration from acceleration time history to velocity and displacement time histories can be conducted using numerical integration methods. The recursive equations for the velocity and displacement at each time step are given in Eqs. (6) and (7) using the trapezoidal rule, respectively.

$$\dot{u}_i = \dot{u}_{i-1} + \frac{1}{2}\Delta t(\ddot{u}_{i-1} + \ddot{u}_i) \quad i = 1, 2, \ldots, N\text{-}1 \qquad \text{(Eq. 6)}$$

$$u_i = u_{i-1} + \frac{1}{2}\Delta t(\dot{u}_{i-1} + \dot{u}_i) = u_{i-1} + \Delta t\dot{u}_{i-1} + \frac{1}{4}\Delta t^2(\ddot{u}_{i-1} + \ddot{u}_i) \quad i = 1, 2, \ldots, N\text{-}1 \qquad \text{(Eq. 7)}$$

in which, $\dot{u}$ and u are the velocity and displacement of the earthquake ground motion; N is the total time points of the acceleration records; and Δt is the time step of the acceleration record.

The numerical integration as shown above will usually incur an unrealistic velocity and displacement offsets from zero at the end of the earthquake record. This is mainly due to recording errors from the accelerometers. To satisfy the fundamental law of physics, the velocity and displacement time histories should retain zero values without permanent velocity and displacement at the end of a simulation period. The baseline correction technique is applied on the filtered acceleration histories to obtain reliable and reasonable velocity and displacement ground motions.

3.2 Modeling of Bridge-traffic Interaction

To formulate interaction forces between the bridge and moving vehicles, the bridge and vehicle wheels are assumed to have point contact without separation. The point contact assumption may not reflect the exact situation when the vehicle wheel is separated from the bridge deck under earthquakes with high intensity. However, it is a necessary mathematical treatment to directly couple the bridge and each individual vehicle in the moving traffic flow given the complexity involved and current constraints of simulation technique. As will be demonstrated in the example, when earthquake excitations are not significantly intensive, the separation of wheels is not significant at most times and the point contact assumption will not cause considerable discrepancy from the realistic situation.

Interaction effects are induced by vehicles in motion under excitations of road surface roughness. Interaction forces at the contact point on the bridge are determined as forces from lower springs and dampers mainly caused by relative movement between the bridge deck and wheel axles (Chen and Cai 2004). The vertical and lateral deformations of the lower vertical and lateral springs and dampers at the k^{th} wheel axle can be expressed as:

$$\Delta^z_{kL(R)} = Z_{akL(R)} - Z_{bkL(R)} - r_{kL(R)} \quad \text{(Eq. 8a)}$$

$$\Delta^y_{kL(R)} = Y_{akL(R)} - Y_{bkL(R)} \quad \text{(Eq. 8b)}$$

in which, $\Delta^z_{kL(R)}$ and $\Delta^y_{kL(R)}$ are vertical and lateral deformations of the lower spring and dampers, respectively; Z and Y are vertical and lateral displacements, respectively; r is the roughness displacement at the bridge contact point; the subscripts a and b indicate wheel axle and bridge contact point, respectively; the subscripts k, $L(R)$ are the wheel axle number and the left (side) of the wheel axle, respectively.

The vertical displacement at the bridge contact point can be expressed by the vertical and torsional displacements of the bridge at the centroid in Eq. (9).

$$Z_{bkL(R)} = h_{bc} + y_{kL(R)}\alpha_{bc} \quad \text{(Eq. 9)}$$

in which, h_{bc} and α_{bc} are the vertical and torsional displacements at the bridge centroid, respectively; $y_{kL(R)}$ is the lateral distance between the contact point and torsional center of the bridge section for the left (right) wheel. Displacements for the bridge and vehicles are measured from deformed positions of the bridge and vehicles under the gravity force, respectively.

The vertical contact force $F^z_{bkL(R)}$ and lateral contact force $F^y_{bkL(R)}$ on the bridge due to the presence of the k^{th} wheel axle at the left (right) side is expressed as:

$$F^z_{bkL(R)} = F^G_{vkL(R)} + K^z_{kL(R)}\Delta^z_{kL(R)} + C^z_{kL(R)}\dot{\Delta}^z_{kL(R)} \quad \text{(Eq. 10a)}$$

$$F^y_{bkL(R)} = K^y_{kL(R)}\Delta^y_{kL(R)} + C^y_{kL(R)}\dot{\Delta}^y_{kL(R)} \quad \text{(Eq. 10b)}$$

in which, $\dot{\Delta}$ is the first derivative of deformation of the relative displacement of the lower spring and damper; K and C are the lower stiffness and damping coefficient.

The vertical contact force $F^z_{vkL(R)}$ and lateral contact force $F^y_{vkL(R)}$ on the k^{th} wheel axle at the left (right) side of the vehicle can be expressed as:

$$F^z_{vkL(R)} = -K^z_{kL(R)}\Delta^z_{kL(R)} - C^z_{kL(R)}\dot{\Delta}^z_{kL(R)} \quad \text{(Eq. 11a)}$$

$$F^y_{vkL(R)} = -K^y_{kL(R)}\Delta^y_{kL(R)} - C^y_{kL(R)}\dot{\Delta}^y_{kL(R)} \quad \text{(Eq. 11b)}$$

Interaction forces between the bridge and vehicles are dependent on motions of the bridge and vehicles. To formulate motion equations of the bridge-vehicle as an interacting system, the motion-dependent parts of bridge-vehicle contact forces are incorporated in equations in the form of coupling matrices.

Motion equations of interacting system of the bridge and vehicles in the stochastic traffic flow are expressed as:

$$\begin{bmatrix} \mathbf{M_b} & \mathbf{0} & \mathbf{0} & \cdots & \mathbf{0} \\ \mathbf{0} & \mathbf{M_{v_1}} & \mathbf{0} & \cdots & \mathbf{0} \\ \mathbf{0} & \mathbf{0} & \mathbf{M_{v_2}} & \cdots & \mathbf{0} \\ \vdots & \vdots & \vdots & \ddots & \vdots \\ \mathbf{0} & \mathbf{0} & \mathbf{0} & \mathbf{0} & \mathbf{M_{v_n}} \end{bmatrix} \begin{Bmatrix} \ddot{\mathbf{U}} \\ \ddot{\mathbf{q}}_1 \\ \ddot{\mathbf{q}}_2 \\ \vdots \\ \ddot{\mathbf{q}}_n \end{Bmatrix} + \begin{bmatrix} \mathbf{C_b} + \sum_{i=1}^{n} \mathbf{C_{bci}} & \mathbf{C_{b,v_1}} & \mathbf{C_{b,v_2}} & \cdots & \mathbf{C_{b,v_n}} \\ \mathbf{C_{v_1,b}} & \mathbf{C_{v_1}} & \mathbf{0} & \cdots & \mathbf{0} \\ \mathbf{C_{v_2,b}} & \mathbf{0} & \mathbf{C_{v_2}} & \cdots & \mathbf{0} \\ \vdots & \vdots & \vdots & \ddots & \vdots \\ \mathbf{C_{v_n,b}} & \mathbf{0} & \mathbf{0} & \cdots & \mathbf{C_{v_n}} \end{bmatrix} \begin{Bmatrix} \dot{\mathbf{U}} \\ \dot{\mathbf{q}}_1 \\ \dot{\mathbf{q}}_2 \\ \vdots \\ \dot{\mathbf{q}}_n \end{Bmatrix}$$
$$+ \begin{bmatrix} \mathbf{K_b} + \sum_{i=1}^{n} \mathbf{K_{bci}} & \mathbf{K_{b,v_1}} & \mathbf{K_{b,v_2}} & \cdots & \mathbf{K_{b,v_n}} \\ \mathbf{K_{v_1,b}} & \mathbf{K_{v_1}} & \mathbf{0} & \cdots & \mathbf{0} \\ \mathbf{K_{v_2,b}} & \mathbf{0} & \mathbf{K_{v_2}} & \cdots & \mathbf{0} \\ \vdots & \vdots & \vdots & \ddots & \vdots \\ \mathbf{K_{v_n,b}} & \mathbf{0} & \mathbf{0} & \cdots & \mathbf{K_{v_n}} \end{bmatrix} \begin{Bmatrix} \mathbf{U} \\ \mathbf{q}_1 \\ \mathbf{q}_2 \\ \vdots \\ \mathbf{q}_n \end{Bmatrix} = \begin{Bmatrix} \sum_{i=1}^{n} \mathbf{F_{v_i}}^{G} + \mathbf{F_b^r} \\ \mathbf{F_{v_1}}^{r} \\ \mathbf{F_{v_2}}^{r} \\ \vdots \\ \mathbf{F_{v_n}}^{r} \end{Bmatrix} \quad \text{(Eq. 12)}$$

in which, $\mathbf{M_b}$, $\mathbf{K_b}$ and $\mathbf{C_b}$ are the mass, stiffness and damping matrices for the bridge structure, respectively; n is the number of vehicles traveling on the roadway-bridge-roadway system in the traffic flow; $\mathbf{M_{v_i}}$, $\mathbf{K_{v_i}}$ and $\mathbf{C_{v_i}}$ are the mass, stiffness and damping matrices of the i^{th} vehicle in the traffic flow, respectively; $\mathbf{K_{bci}}$ and $\mathbf{C_{bci}}$ are the stiffness and damping contributions to the bridge structure due to coupling effects between the i^{th} vehicle in the traffic flow and the bridge, respectively, which can be obtained from stiffness $\mathbf{K_{bci}^{kL(R)}}$ and damping $\mathbf{C_{bci}^{kL(R)}}$ coupling matrix of the k^{th} wheel set at the left (right) side for the i^{th} vehicle, corresponding to vertical, lateral and rotational degrees of freedom of the bridge for the 1st, 2nd and 3rd row or column, respectively;

$$\mathbf{K_{bci}^{kL(R)}} = \begin{bmatrix} K_{kL(R)}^{z} & 0 & 0 \\ 0 & K_{kL(R)}^{y} & 0 \\ 0 & 0 & K_{kL(R)}^{z} \cdot y_{kL(R)} \end{bmatrix} \quad \text{(Eq. 13a)}$$

$$\mathbf{C_{bci}^{kL(R)}} = \begin{bmatrix} C_{kL(R)}^{z} & 0 & 0 \\ 0 & C_{kL(R)}^{y} & 0 \\ 0 & 0 & C_{kL(R)}^{z} \cdot y_{kL(R)} \end{bmatrix} \quad \text{(Eq. 13b)}$$

$\mathbf{K_{b,v_i}}$ and $\mathbf{C_{b,v_i}}$ are the coupled stiffness and damping matrices for the bridge structure due to motion of the i^{th} vehicle in the traffic flow, respectively, which can be obtained from stiffness and damping coupling terms of the k^{th} wheel wheel set at the left (right) side for the i^{th} vehicle, corresponding to the vertical, lateral and rotational degrees of freedom of the bridge for the 1st, 2nd and 3rd row or column, respectively;

$$\mathbf{K_{b,v_i}^{kL(R)}} = \begin{bmatrix} -K_{kL(R)}^{z} & 0 & 0 \\ 0 & -K_{kL(R)}^{y} & 0 \\ 0 & 0 & -K_{kL(R)}^{z} \cdot y_{kL(R)} \end{bmatrix} \quad \text{(Eq. 14a)}$$

$$\mathbf{C_{b,v_i}^{kL(R)}} = \begin{bmatrix} -C_{kL(R)}^{z} & 0 & 0 \\ 0 & -C_{kL(R)}^{y} & 0 \\ 0 & 0 & -C_{kL(R)}^{z} \cdot y_{kL(R)} \end{bmatrix} \quad \text{(Eq. 14b)}$$

$\mathbf{K_{v_i,b}}$ and $\mathbf{C_{v_i,b}}$ are the coupled stiffness and damping matrices for the i^{th} vehicle in the traffic flow due to motion of the bridge, which are equal to the transposed matrices of $\mathbf{K_{b,v_i}}$ and $\mathbf{C_{b,v_i}}$, respectively; $\mathbf{U}$ is the

bridge response vector; $\mathbf{q_i}$ (i = 1, 2, …, n) is the response vector of the i^{th} vehicle in the traffic flow; One-dot and two-dot superscripts of the displacement vector denote the velocity and acceleration, respectively; $\mathbf{F}_{v_i}^{G}$ is the gravity force of the i^{th} vehicle; $\mathbf{F}_{b}^{r}$ and $\mathbf{F}_{v_i}^{r}$ are the forces on the bridge and the i^{th} vehicle due to road surface roughness, respectively. The bridge-traffic interaction model is developed using programming language MATLAB.

3.3 Modeling of the Coupled Bridge-traffic System under Seismic Excitations

Traditionally, bridge seismic analysis is conducted on the bridge structure without considering interactions between the bridge and moving vehicles. Considering that an earthquake usually strikes suddenly and lasts for a short period of time, drivers may not have enough time to realize the occurrence and accordingly respond on vehicle maneuver timely. The actual driving behavior change subjected to earthquake is complicated in nature and there is currently no appropriate model that can characterize such driving behavior. Therefore, in the present study, the change of driving behavior is not considered, and the traffic flow pattern is assumed not to be affected by the earthquake events.

When an earthquake event strikes the bridge site, interactions between the bridge and vehicles will not only be influenced by the seismic excitations through the bridge supports, but they also affect earthquake forces acting on the bridge and vehicles. Therefore, the seismic analysis on the bridge-traffic interaction system should take into account the influence between bridge-traffic interaction and exerted earthquake loads on the bridge. Since earthquake record is usually obtained from accelerometers, the direct use of seismic loading, in terms of acceleration histories, would be the natural and preferred choice in seismic analysis compared to the displacement seismic loading method.

The study proposes a methodology based on the acceleration seismic-loading approach and considers bridge-traffic interaction effects on seismic forces at the same time. Because the bridge supports on the ground experience motions due to earthquakes, the DOFs on the bridge are partitioned into unconstrained DOFs on the bridge structure and constrained DOFs at the supports. The methodology starts with equations of motion on the bridge structure with unconstrained DOFs, bridge constrained DOFs at the supports and each individual vehicle in the traffic flow under earthquake excitations, as shown in Eq. (15).

$$\begin{bmatrix} \mathbf{M}_{bu} & \mathbf{0} & \mathbf{0} & \mathbf{0} & \cdots & \mathbf{0} \\ \mathbf{0} & \mathbf{M}_{bg} & \mathbf{0} & \mathbf{0} & \cdots & \mathbf{0} \\ \mathbf{0} & \mathbf{0} & \mathbf{M}_{v_1} & \mathbf{0} & \cdots & \mathbf{0} \\ \mathbf{0} & \mathbf{0} & \mathbf{0} & \mathbf{M}_{v_2} & \cdots & \mathbf{0} \\ \vdots & \vdots & \vdots & \vdots & \ddots & \vdots \\ \mathbf{0} & \mathbf{0} & \mathbf{0} & \mathbf{0} & \mathbf{0} & \mathbf{M}_{v_n} \end{bmatrix} \begin{Bmatrix} \ddot{\mathbf{U}} \\ \ddot{\mathbf{u}} \\ \ddot{\mathbf{q}}_1 \\ \ddot{\mathbf{q}}_2 \\ \vdots \\ \ddot{\mathbf{q}}_n \end{Bmatrix} + \begin{bmatrix} \mathbf{C}_{bu} + \sum_{i=1}^{n} \mathbf{C}_{bci} & \mathbf{C}_{bg,u} & \mathbf{C}_{b,v_1} & \mathbf{C}_{b,v_2} & \cdots & \mathbf{C}_{b,v_n} \\ \mathbf{C}_{bu,g} & \mathbf{C}_{bg} & \mathbf{0} & \mathbf{0} & \cdots & \mathbf{0} \\ \mathbf{C}_{v_1,b} & \mathbf{0} & \mathbf{C}_{v_1} & \mathbf{0} & \cdots & \mathbf{0} \\ \mathbf{C}_{v_2,b} & \mathbf{0} & \mathbf{0} & \mathbf{C}_{v_2} & \cdots & \mathbf{0} \\ \vdots & \vdots & \vdots & \vdots & \ddots & \vdots \\ \mathbf{C}_{v_n,b} & \mathbf{0} & \mathbf{0} & \mathbf{0} & \cdots & \mathbf{C}_{v_n} \end{bmatrix} \begin{Bmatrix} \dot{\mathbf{U}} \\ \dot{\mathbf{u}} \\ \dot{\mathbf{q}}_1 \\ \dot{\mathbf{q}}_2 \\ \vdots \\ \dot{\mathbf{q}}_n \end{Bmatrix}$$

$$+ \begin{bmatrix} \mathbf{K}_{bu} + \sum_{i=1}^{n} \mathbf{K}_{bci} & \mathbf{K}_{bg,u} & \mathbf{K}_{b,v_1} & \mathbf{K}_{b,v_2} & \cdots & \mathbf{K}_{b,v_n} \\ \mathbf{K}_{bu,g} & \mathbf{K}_{bg} & \mathbf{0} & \mathbf{0} & \cdots & \mathbf{0} \\ \mathbf{K}_{v_1,b} & \mathbf{0} & \mathbf{K}_{v_1} & \mathbf{0} & \cdots & \mathbf{0} \\ \mathbf{K}_{v_2,b} & \mathbf{0} & \mathbf{0} & \mathbf{K}_{v_2} & \cdots & \mathbf{0} \\ \vdots & \vdots & \vdots & \vdots & \ddots & \vdots \\ \mathbf{K}_{v_n,b} & \mathbf{0} & \mathbf{0} & \mathbf{0} & \cdots & \mathbf{K}_{v_n} \end{bmatrix} \begin{Bmatrix} \mathbf{U} \\ \mathbf{u} \\ \mathbf{q}_1 \\ \mathbf{q}_2 \\ \vdots \\ \mathbf{q}_n \end{Bmatrix} = \begin{Bmatrix} \sum_{i=1}^{n} \mathbf{F}_{v_1}^{G} + \mathbf{F}_{b}^{r} \\ \mathbf{F}_{g} \\ \mathbf{F}_{v_1}^{r} \\ \mathbf{F}_{v_2}^{r} \\ \vdots \\ \mathbf{F}_{v_n}^{r} \end{Bmatrix} \quad \text{(Eq. 15)}$$

in which, u is the support displacement vector at the bridge constrained DOFs, which contains three variables corresponding to support displacements in the longitudinal, transverse and vertical directions respectively, where $\mathbf{M_{bg}}$, $\mathbf{K_{bg}}$ and $\mathbf{C_{bg}}$ are the mass, stiffness and damping matrices of the bridge structure corresponding to the constrained DOFs, respectively; $\mathbf{K_{bu,g}}$ and $\mathbf{K_{bg,u}}$ are the coupled stiffness matrices of the bridge structure corresponding to the constrained and unconstrained DOFs, respectively; $\mathbf{C_{bu,g}}$ and $\mathbf{C_{bg,u}}$ are the coupled damping matrices of the bridge structure corresponding to the constrained and unconstrained DOFs, respectively; $\mathbf{F_g}$ is the reaction force at the supports.

Total response of the bridge is divided into the pseudo-static part and dynamic part following the relative motion method (Léger, 1990), which is shown in Eq. (16).

$$\mathbf{U} = \mathbf{U^s} + \mathbf{U^d} \tag{Eq. 16}$$

Equilibrium equations of the bridge structure of the unconstrained DOFs and constrained DOFs can be given in the following form:

$$\begin{bmatrix} \mathbf{K_{bu}} & \mathbf{K_{bg,u}} \\ \mathbf{K_{bu,g}} & \mathbf{K_{bg}} \end{bmatrix} \begin{Bmatrix} \mathbf{U^s} \\ \mathbf{u} \end{Bmatrix} = \begin{Bmatrix} \mathbf{0} \\ \mathbf{F_g^s} \end{Bmatrix} \tag{Eq. 17}$$

in which, F_g^s is the pseudo-static reaction force at the supports. The first equation can be rewritten in the form shown in Eq. (18):

$$\mathbf{K_{bu}U^s + K_{bg,u}u = 0} \tag{Eq. 18}$$

By defining the influence matrix R, the pseudo-static response can be expressed through support displacement vector u and the influence matrix. The pseudo-static response is obtained from static analysis at each time step and therefore it varies with respect to time.

$$\mathbf{U^s} = -\mathbf{K_{bu}^{-1}K_{bg,u}u} = \mathbf{Ru} \tag{Eq. 19}$$

From the first row of Eq. (15), the equation of motion corresponding to the bridge unconstrained DOFs can be written as:

$$\begin{aligned} &\mathbf{M_{bu}}\ddot{\mathbf{U}}^{\mathbf{d}} + (\mathbf{C_{bu}} + \textstyle\sum_{i=1}^{n}\mathbf{C_{bci}})\dot{\mathbf{U}}^{\mathbf{d}} + (\mathbf{K_{bu}} + \textstyle\sum_{i=1}^{n}\mathbf{K_{bci}})\mathbf{U}^{\mathbf{d}} \\ &= -\mathbf{M_{bu}}\ddot{\mathbf{U}}^{\mathbf{s}} - (\mathbf{C_{bu}} + \textstyle\sum_{i=1}^{n}\mathbf{C_{bci}})\dot{\mathbf{U}}^{\mathbf{s}} - (\mathbf{K_{bu}} + \textstyle\sum_{i=1}^{n}\mathbf{K_{bci}})\mathbf{U}^{\mathbf{s}} - \mathbf{C_{bg,u}}\dot{\mathbf{u}} - \mathbf{K_{bg,u}}\mathbf{u} - \textstyle\sum_{i=1}^{n}\mathbf{C_{b,v_i}}\dot{\mathbf{q}}_{\mathbf{i}} - \textstyle\sum_{i=1}^{n}\mathbf{K_{b,v_i}}\dot{\mathbf{q}}_{\mathbf{i}} + \textstyle\sum_{i=1}^{n}\mathbf{F_{v_i}}^{\mathbf{G}} + \mathbf{F_b^r} \\ &= -\mathbf{M_{bu}R}\ddot{\mathbf{u}} - \mathbf{C_{bu}R}\dot{\mathbf{u}} - \mathbf{C_{bg,u}}\dot{\mathbf{u}} - \textstyle\sum_{i=1}^{n}\mathbf{C_{bci}R}\dot{\mathbf{u}} - \textstyle\sum_{i=1}^{n}\mathbf{K_{bci}Ru} - \textstyle\sum_{i=1}^{n}\mathbf{C_{b,v_i}}\dot{\mathbf{q}}_{\mathbf{i}} - \textstyle\sum_{i=1}^{n}\mathbf{K_{b,v_i}}\dot{\mathbf{q}}_{\mathbf{i}} + \textstyle\sum_{i=1}^{n}\mathbf{F_{v_i}}^{\mathbf{G}} + \mathbf{F_b^r} \end{aligned} \tag{Eq. 20}$$

Items containing earthquake ground motion in the form of acceleration, velocity and displacement are defined as components of total equivalent earthquake force on the bridge unconstrained DOFs, as shown in Eq. (21).

$$\mathbf{F_{bu}^{eq}} = -\mathbf{M_{bu}R}\ddot{\mathbf{u}} - \mathbf{C_{bu}R}\dot{\mathbf{u}} - \mathbf{C_{bg,u}}\dot{\mathbf{u}} - \textstyle\sum_{i=1}^{n}\mathbf{C_{bci}R}\dot{\mathbf{u}} - \textstyle\sum_{i=1}^{n}\mathbf{K_{bci}Ru} = \mathbf{F_{bu}^{eq,t}} + \mathbf{F_{bu}^{eq,c}} \tag{Eq. 21a}$$

in which, the traditional earthquake force $F_{bu}^{eq,t}$ and the coupled earthquake force $F_{bu}^{eq,c}$ due to the coupling between earthquake and traffic are defined in the following equations:

$$\mathbf{F}_{\mathbf{bu}}^{\mathbf{eq,t}} = -\mathbf{M}_{\mathbf{bu}}\mathbf{R}\ddot{\mathbf{u}} - \mathbf{C}_{\mathbf{bu}}\mathbf{R}\dot{\mathbf{u}} - \mathbf{C}_{\mathbf{bg,u}}\dot{\mathbf{u}} \quad \text{(Eq. 21b)}$$

$$\mathbf{F}_{\mathbf{bu}}^{\mathbf{eq,c}} = -\sum_{\mathbf{i=1}}^{\mathbf{n}}\mathbf{C}_{\mathbf{bci}}\mathbf{R}\dot{\mathbf{u}} - \sum_{\mathbf{i=1}}^{\mathbf{n}}\mathbf{K}_{\mathbf{bci}}\mathbf{R}\mathbf{u} \quad \text{(Eq. 21c)}$$

The coupled earthquake force reflects the new term that is due to the bridge-traffic interactions and was usually ignored in most existing studies. The second and third terms in the traditional earthquake force $F_{bu}^{eq,t}$ are usually very small as compared to the first term, and therefore are ignored following current seismic analysis practice. From the $(i+2)^{th}$ row of the equations of motion in Eq. (15), the equation of motion corresponding to the i^{th} vehicle can be written as:

$$\mathbf{M}_{\mathbf{v_i}}\ddot{\mathbf{q}}_{\mathbf{i}} + \mathbf{C}_{\mathbf{v_i,b}}\dot{\mathbf{U}}^{\mathbf{d}} + \mathbf{K}_{\mathbf{v_i,b}}\mathbf{U}^{\mathbf{d}} + \mathbf{C}_{\mathbf{v_i}}\dot{\mathbf{q}}_{\mathbf{i}} + \mathbf{K}_{\mathbf{v_i}}\mathbf{q}_{\mathbf{i}} = -\mathbf{C}_{\mathbf{v_i,b}}\dot{\mathbf{U}}^{\mathbf{s}} - \mathbf{K}_{\mathbf{v_i,b}}\mathbf{U}^{\mathbf{s}} + \mathbf{F}_{\mathbf{v_i}}{}^{\mathbf{r}} = -\mathbf{C}_{\mathbf{v_i,b}}\mathbf{R}\dot{\mathbf{u}} - \mathbf{K}_{\mathbf{v_i,b}}\mathbf{R}\mathbf{u} + \mathbf{F}_{\mathbf{v_i}}{}^{\mathbf{r}} \quad \text{(Eq. 22)}$$

Similarly, the total equivalent earthquake force on the i^{th} vehicle is defined in Eq. (23), which contains only coupled earthquake force.

$$\mathbf{F}_{\mathbf{v_i}}^{\mathbf{eq}} = -\mathbf{C}_{\mathbf{v_i,b}}\mathbf{R}\dot{\mathbf{u}} - \mathbf{K}_{\mathbf{v_i,b}}\mathbf{R}\mathbf{u} \quad \text{(Eq. 23)}$$

After substituting the total equivalent earthquake force on the bridge and each vehicle into the equations of motion, the equation of motion corresponding to the bridge unconstrained degrees of freedom can be rewritten as:

$$\begin{aligned}
&\mathbf{M}_{\mathbf{bu}}\ddot{\mathbf{U}}^{\mathbf{d}} + (\mathbf{C}_{\mathbf{bu}} + \sum_{\mathbf{i=1}}^{\mathbf{n}}\mathbf{C}_{\mathbf{bci}})\dot{\mathbf{U}}^{\mathbf{d}} + (\mathbf{K}_{\mathbf{bu}} + \sum_{\mathbf{i=1}}^{\mathbf{n}}\mathbf{K}_{\mathbf{bci}})\mathbf{U}^{\mathbf{d}} \\
&= -\mathbf{M}_{\mathbf{bu}}\ddot{\mathbf{U}}^{\mathbf{s}} - (\mathbf{C}_{\mathbf{bu}} + \sum_{\mathbf{i=1}}^{\mathbf{n}}\mathbf{C}_{\mathbf{bci}})\dot{\mathbf{U}}^{\mathbf{s}} - (\mathbf{K}_{\mathbf{bu}} + \sum_{\mathbf{i=1}}^{\mathbf{n}}\mathbf{K}_{\mathbf{bci}})\mathbf{U}^{\mathbf{s}} - \mathbf{C}_{\mathbf{bg,u}}\dot{\mathbf{u}} - \mathbf{K}_{\mathbf{bg,u}}\mathbf{u} - \sum_{\mathbf{i=1}}^{\mathbf{n}}\mathbf{C}_{\mathbf{b,v_i}}\dot{\mathbf{q}}_{\mathbf{i}} - \sum_{\mathbf{i=1}}^{\mathbf{n}}\mathbf{K}_{\mathbf{b,v_i}}\dot{\mathbf{q}}_{\mathbf{i}} + \sum_{\mathbf{i=1}}^{\mathbf{n}}\mathbf{F}_{\mathbf{v_i}}{}^{\mathbf{G}} + \mathbf{F}_{\mathbf{b}}^{\mathbf{r}} \\
&= \mathbf{F}_{\mathbf{bu}}^{\mathbf{eq}} - \sum_{\mathbf{i=1}}^{\mathbf{n}}\mathbf{C}_{\mathbf{b,v_i}}\dot{\mathbf{q}}_{\mathbf{i}} - \sum_{\mathbf{i=1}}^{\mathbf{n}}\mathbf{K}_{\mathbf{b,v_i}}\dot{\mathbf{q}}_{\mathbf{i}} + \sum_{\mathbf{i=1}}^{\mathbf{n}}\mathbf{F}_{\mathbf{v_i}}{}^{\mathbf{G}} + \mathbf{F}_{\mathbf{b}}^{\mathbf{r}}
\end{aligned} \quad \text{(Eq. 24)}$$

The equation of motion corresponding to the i^{th} vehicle can be written as:

$$\mathbf{M}_{\mathbf{v_i}}\ddot{\mathbf{q}}_{\mathbf{i}} + \mathbf{C}_{\mathbf{v_i,b}}\dot{\mathbf{x}}^{\mathbf{d}} + \mathbf{K}_{\mathbf{v_i,b}}\mathbf{x}^{\mathbf{d}} + \mathbf{C}_{\mathbf{v_i}}\dot{\mathbf{q}}_{\mathbf{i}} + \mathbf{K}_{\mathbf{v_i}}\mathbf{q}_{\mathbf{i}} = \mathbf{F}_{\mathbf{v_i}}^{\mathbf{eq}} + \mathbf{F}_{\mathbf{v_i}}{}^{\mathbf{r}} \quad \text{(Eq. 25)}$$

Motion-dependent components in the force vector are reformulated on the left side of equations of motion. Then equations of motion of the bridge-traffic system can be reduced without including the bridge constrained DOFs on the ground in the following matrix form in Eq. (26):

$$\begin{bmatrix} \mathbf{M}_{bu} & \mathbf{0} & \mathbf{0} & \cdots & \mathbf{0} \\ \mathbf{0} & \mathbf{M}_{v_1} & \mathbf{0} & \cdots & \mathbf{0} \\ \mathbf{0} & \mathbf{0} & \mathbf{M}_{v_2} & \cdots & \mathbf{0} \\ \vdots & \vdots & \vdots & \ddots & \vdots \\ \mathbf{0} & \mathbf{0} & \mathbf{0} & \mathbf{0} & \mathbf{M}_{v_n} \end{bmatrix} \begin{Bmatrix} \ddot{\mathbf{U}}^{\mathbf{d}} \\ \ddot{\mathbf{q}}_1 \\ \ddot{\mathbf{q}}_2 \\ \vdots \\ \ddot{\mathbf{q}}_n \end{Bmatrix} + \begin{bmatrix} \mathbf{C}_{bu} + \sum_{i=1}^{n} \mathbf{C}_{bci} & \mathbf{C}_{b,v_1} & \mathbf{C}_{b,v_2} & \cdots & \mathbf{C}_{b,v_n} \\ \mathbf{C}_{v_1,b} & \mathbf{C}_{v_1} & \mathbf{0} & \cdots & \mathbf{0} \\ \mathbf{C}_{v_2,b} & \mathbf{0} & \mathbf{C}_{v_2} & \cdots & \mathbf{0} \\ \vdots & \vdots & \vdots & \ddots & \vdots \\ \mathbf{C}_{v_n,b} & \mathbf{0} & \mathbf{0} & \cdots & \mathbf{C}_{v_n} \end{bmatrix} \begin{Bmatrix} \dot{\mathbf{U}}^{\mathbf{d}} \\ \dot{\mathbf{q}}_1 \\ \dot{\mathbf{q}}_2 \\ \vdots \\ \dot{\mathbf{q}}_n \end{Bmatrix}$$
$$+ \begin{bmatrix} \mathbf{K}_{bu} + \sum_{i=1}^{n} \mathbf{K}_{bci} & \mathbf{K}_{b,v_1} & \mathbf{K}_{b,v_2} & \cdots & \mathbf{K}_{b,v_n} \\ \mathbf{K}_{v_1,b} & \mathbf{K}_{v_1} & \mathbf{0} & \cdots & \mathbf{0} \\ \mathbf{K}_{v_2,b} & \mathbf{0} & \mathbf{K}_{v_2} & \cdots & \mathbf{0} \\ \vdots & \vdots & \vdots & \ddots & \vdots \\ \mathbf{K}_{v_n,b} & \mathbf{0} & \mathbf{0} & \cdots & \mathbf{K}_{v_n} \end{bmatrix} \begin{Bmatrix} \mathbf{U}^{\mathbf{d}} \\ \mathbf{q}_1 \\ \mathbf{q}_2 \\ \vdots \\ \mathbf{q}_n \end{Bmatrix} = \begin{Bmatrix} \mathbf{F}_{bu}^{eq} + \sum_{i=1}^{n} \mathbf{F}_{v_i}^{G} + \mathbf{F}_b^r \\ \mathbf{F}_{v_1}^{eq} + \mathbf{F}_{v_1}^{r} \\ \mathbf{F}_{v_2}^{eq} + \mathbf{F}_{v_2}^{r} \\ \vdots \\ \mathbf{F}_{v_n}^{eq} + \mathbf{F}_{v_n}^{r} \end{Bmatrix} \quad \text{(Eq. 26)}$$

It can be seen in Eq. (26) that earthquake excitations at the bridge supports have dynamic effects on the bridge and individual vehicles, which are related to interactions between the bridge and vehicles. The mode superposition approach is further used in the proposed method by selecting a certain number of participating modes on the bridge. Through the mode superposition approach, dynamic displacement of the bridge can be decomposed into mode shape matrix and generalized coordinates.

$$\mathbf{U}^{\mathbf{d}} = \sum_{j=1}^{m} \boldsymbol{\varphi}_j \xi_j = [\boldsymbol{\varphi}_1 \boldsymbol{\varphi}_2 \ldots \boldsymbol{\varphi}_m] \{\xi_1 \xi_2 \ldots \xi_m\}^T = \boldsymbol{\Phi} \boldsymbol{\xi}^{\mathbf{d}} \quad \text{(Eq. 27)}$$

in which, m is the number of the selected modes involved in the analysis; $\boldsymbol{\Phi}$ is the mode shape matrix; $\boldsymbol{\xi}^{\mathbf{d}}$ is the vector of the generalized coordinates.

Following traditional multi-mode analysis procedure, Eq. (26) with physical coordinates can be converted to those with generalized coordinates of the bridge structure:

$$\begin{bmatrix} \boldsymbol{\Phi}^T \mathbf{M}_{bu} \boldsymbol{\Phi} & \mathbf{0} & \mathbf{0} & \cdots & \mathbf{0} \\ \mathbf{0} & \mathbf{M}_{v_1} & \mathbf{0} & \cdots & \mathbf{0} \\ \mathbf{0} & \mathbf{0} & \mathbf{M}_{v_2} & \cdots & \mathbf{0} \\ \vdots & \vdots & \vdots & \ddots & \vdots \\ \mathbf{0} & \mathbf{0} & \mathbf{0} & \mathbf{0} & \mathbf{M}_{v_n} \end{bmatrix} \begin{Bmatrix} \ddot{\boldsymbol{\xi}}^{\mathbf{d}} \\ \ddot{\mathbf{q}}_1 \\ \ddot{\mathbf{q}}_2 \\ \vdots \\ \ddot{\mathbf{q}}_n \end{Bmatrix} + \begin{bmatrix} \boldsymbol{\Phi}^T \mathbf{C}_{bu} \boldsymbol{\Phi} + \boldsymbol{\Phi}^T \sum_{i=1}^{n} \mathbf{C}_{bci} \boldsymbol{\Phi} & \boldsymbol{\Phi}^T \mathbf{C}_{b,v_1} & \boldsymbol{\Phi}^T \mathbf{C}_{b,v_2} & \cdots & \boldsymbol{\Phi}^T \mathbf{C}_{b,v_n} \\ \mathbf{C}_{v_1,b} \boldsymbol{\Phi} & \mathbf{C}_{v_1} & \mathbf{0} & \cdots & \mathbf{0} \\ \mathbf{C}_{v_2,b} \boldsymbol{\Phi} & \mathbf{0} & \mathbf{C}_{v_2} & \cdots & \mathbf{0} \\ \vdots & \vdots & \vdots & \ddots & \vdots \\ \mathbf{C}_{v_n,b} \boldsymbol{\Phi} & \mathbf{0} & \mathbf{0} & \cdots & \mathbf{C}_{v_n} \end{bmatrix} \begin{Bmatrix} \dot{\boldsymbol{\xi}}^{\mathbf{d}} \\ \dot{\mathbf{q}}_1 \\ \dot{\mathbf{q}}_2 \\ \vdots \\ \dot{\mathbf{q}}_n \end{Bmatrix}$$
$$+ \begin{bmatrix} \boldsymbol{\Phi}^T \mathbf{K}_{bu} \boldsymbol{\Phi} + \boldsymbol{\Phi}^T \sum_{i=1}^{n} \mathbf{K}_{bci} \boldsymbol{\Phi} & \boldsymbol{\Phi}^T \mathbf{K}_{b,v_1} & \boldsymbol{\Phi}^T \mathbf{K}_{b,v_2} & \cdots & \boldsymbol{\Phi}^T \mathbf{K}_{b,v_n} \\ \mathbf{K}_{v_1,b} \boldsymbol{\Phi} & \mathbf{K}_{v_1} & \mathbf{0} & \cdots & \mathbf{0} \\ \mathbf{K}_{v_2,b} \boldsymbol{\Phi} & \mathbf{0} & \mathbf{K}_{v_2} & \cdots & \mathbf{0} \\ \vdots & \vdots & \vdots & \ddots & \vdots \\ \mathbf{K}_{v_n,b} \boldsymbol{\Phi} & \mathbf{0} & \mathbf{0} & \cdots & \mathbf{K}_{v_n} \end{bmatrix} \begin{Bmatrix} \boldsymbol{\xi}^{\mathbf{d}} \\ \mathbf{q}_1 \\ \mathbf{q}_2 \\ \vdots \\ \mathbf{q}_n \end{Bmatrix} = \begin{Bmatrix} \boldsymbol{\Phi}^T \mathbf{F}_{bu}^{eq} + \boldsymbol{\Phi}^T \sum_{i=1}^{n} \mathbf{F}_{v_i}^{G} + \boldsymbol{\Phi}^T \mathbf{F}_b^r \\ \mathbf{F}_{v_1}^{eq} + \mathbf{F}_{v_1}^{r} \\ \mathbf{F}_{v_2}^{eq} + \mathbf{F}_{v_2}^{r} \\ \vdots \\ \mathbf{F}_{v_n}^{eq} + \mathbf{F}_{v_n}^{r} \end{Bmatrix} \quad \text{(Eq. 28)}$$

Stiffness and damping matrices of the bridge structure can be expressed as functions of the mass matrix and modal properties, as shown in Eq. (29a) and (29b), respectively.

$$\boldsymbol{\varphi}_j^T \mathbf{K}_{bu} \boldsymbol{\varphi}_j = \omega_j^2 \boldsymbol{\varphi}_j^T \mathbf{M}_{bu} \boldsymbol{\varphi}_j \quad \text{(Eq. 29a)}$$

$$\boldsymbol{\varphi}_j^T \mathbf{C}_{bu} \boldsymbol{\varphi}_j = 2\omega_j \eta_j \boldsymbol{\varphi}_j^T \mathbf{M}_{bu} \boldsymbol{\varphi}_j \quad \text{(Eq. 29b)}$$

By applying these equations, the final equations of motion in terms of modal coordinates for the bridge structure can be formulated in Eq. (30).

$$\begin{bmatrix} \boldsymbol{\varphi}_1^{\mathrm{T}}\mathbf{M}_{\mathrm{bu}}\boldsymbol{\varphi}_1 & \mathbf{0} & \cdots & \mathbf{0} & \mathbf{0} & \mathbf{0} & \cdots & \mathbf{0} \\ \mathbf{0} & \boldsymbol{\varphi}_2^{\mathrm{T}}\mathbf{M}_{\mathrm{bu}}\boldsymbol{\varphi}_2 & \cdots & \mathbf{0} & \mathbf{0} & \mathbf{0} & \cdots & \mathbf{0} \\ \vdots & \vdots & \ddots & \mathbf{0} & \mathbf{0} & \mathbf{0} & \cdots & \mathbf{0} \\ \mathbf{0} & \mathbf{0} & \cdots & \boldsymbol{\varphi}_m^{\mathrm{T}}\mathbf{M}_{\mathrm{bu}}\boldsymbol{\varphi}_m & \mathbf{0} & \mathbf{0} & \cdots & \mathbf{0} \\ \mathbf{0} & \mathbf{0} & \mathbf{0} & \mathbf{0} & \mathbf{M}_{\mathrm{v}_1} & \mathbf{0} & \cdots & \mathbf{0} \\ \mathbf{0} & \mathbf{0} & \mathbf{0} & \mathbf{0} & \mathbf{0} & \mathbf{M}_{\mathrm{v}_2} & \cdots & \mathbf{0} \\ \vdots & \vdots & \vdots & \vdots & \vdots & \vdots & \ddots & \vdots \\ \mathbf{0} & \mathbf{0} & \mathbf{0} & \mathbf{0} & \mathbf{0} & \mathbf{0} & \cdots & \mathbf{M}_{\mathrm{v}_n} \end{bmatrix} \begin{Bmatrix} \ddot{\boldsymbol{\xi}}_1^{\mathrm{d}} \\ \ddot{\boldsymbol{\xi}}_2^{\mathrm{d}} \\ \vdots \\ \ddot{\boldsymbol{\xi}}_m^{\mathrm{d}} \\ \ddot{\mathbf{q}}_1 \\ \ddot{\mathbf{q}}_2 \\ \vdots \\ \ddot{\mathbf{q}}_n \end{Bmatrix} + \begin{bmatrix} \boldsymbol{\Theta}_{\mathrm{C}}^1 & \mathbf{0} & \cdots & \mathbf{0} & \boldsymbol{\varphi}_1^{\mathrm{T}}\mathbf{C}_{\mathrm{b},\mathrm{v}_1} & \boldsymbol{\varphi}_1^{\mathrm{T}}\mathbf{C}_{\mathrm{b},\mathrm{v}_2} & \cdots & \boldsymbol{\varphi}_1^{\mathrm{T}}\mathbf{C}_{\mathrm{b},\mathrm{v}_n} \\ \mathbf{0} & \boldsymbol{\Theta}_{\mathrm{C}}^2 & \cdots & \mathbf{0} & \boldsymbol{\varphi}_2^{\mathrm{T}}\mathbf{C}_{\mathrm{b},\mathrm{v}_1} & \boldsymbol{\varphi}_2^{\mathrm{T}}\mathbf{C}_{\mathrm{b},\mathrm{v}_2} & \cdots & \boldsymbol{\varphi}_2^{\mathrm{T}}\mathbf{C}_{\mathrm{b},\mathrm{v}_n} \\ \vdots & \vdots & \ddots & \vdots & \vdots & \vdots & \vdots & \vdots \\ \mathbf{0} & \mathbf{0} & \cdots & \boldsymbol{\Theta}_{\mathrm{C}}^m & \boldsymbol{\varphi}_m^{\mathrm{T}}\mathbf{C}_{\mathrm{b},\mathrm{v}_1} & \boldsymbol{\varphi}_m^{\mathrm{T}}\mathbf{C}_{\mathrm{b},\mathrm{v}_2} & \cdots & \boldsymbol{\varphi}_m^{\mathrm{T}}\mathbf{C}_{\mathrm{b},\mathrm{v}_n} \\ \mathbf{C}_{\mathrm{v}_1,\mathrm{b}}\boldsymbol{\varphi}_1 & \mathbf{C}_{\mathrm{v}_1,\mathrm{b}}\boldsymbol{\varphi}_2 & \cdots & \mathbf{C}_{\mathrm{v}_1,\mathrm{b}}\boldsymbol{\varphi}_m & \mathbf{C}_{\mathrm{v}_1} & \mathbf{0} & \cdots & \mathbf{0} \\ \mathbf{C}_{\mathrm{v}_2,\mathrm{b}}\boldsymbol{\varphi}_1 & \mathbf{C}_{\mathrm{v}_2,\mathrm{b}}\boldsymbol{\varphi}_2 & \cdots & \mathbf{C}_{\mathrm{v}_2,\mathrm{b}}\boldsymbol{\varphi}_m & \mathbf{0} & \mathbf{C}_{\mathrm{v}_2} & \cdots & \mathbf{0} \\ \vdots & \vdots & \vdots & \vdots & \vdots & \vdots & \ddots & \vdots \\ \mathbf{C}_{\mathrm{v}_n,\mathrm{b}}\boldsymbol{\varphi}_1 & \mathbf{C}_{\mathrm{v}_n,\mathrm{b}}\boldsymbol{\varphi}_2 & \cdots & \mathbf{C}_{\mathrm{v}_n,\mathrm{b}}\boldsymbol{\varphi}_m & \mathbf{0} & \mathbf{0} & \cdots & \mathbf{C}_{\mathrm{v}_n} \end{bmatrix} \begin{Bmatrix} \dot{\boldsymbol{\xi}}_1^{\mathrm{d}} \\ \dot{\boldsymbol{\xi}}_2^{\mathrm{d}} \\ \vdots \\ \dot{\boldsymbol{\xi}}_m^{\mathrm{d}} \\ \dot{\mathbf{q}}_1 \\ \dot{\mathbf{q}}_2 \\ \vdots \\ \dot{\mathbf{q}}_n \end{Bmatrix} +$$

$$\begin{bmatrix} \boldsymbol{\Theta}_{\mathrm{K}}^1 & \mathbf{0} & \cdots & \mathbf{0} & \boldsymbol{\varphi}_1^{\mathrm{T}}\mathbf{K}_{\mathrm{b},\mathrm{v}_1} & \boldsymbol{\varphi}_1^{\mathrm{T}}\mathbf{K}_{\mathrm{b},\mathrm{v}_2} & \cdots & \boldsymbol{\varphi}_1^{\mathrm{T}}\mathbf{K}_{\mathrm{b},\mathrm{v}_n} \\ \mathbf{0} & \boldsymbol{\Theta}_{\mathrm{K}}^2 & \cdots & \mathbf{0} & \boldsymbol{\varphi}_2^{\mathrm{T}}\mathbf{K}_{\mathrm{b},\mathrm{v}_1} & \boldsymbol{\varphi}_2^{\mathrm{T}}\mathbf{K}_{\mathrm{b},\mathrm{v}_2} & \cdots & \boldsymbol{\varphi}_2^{\mathrm{T}}\mathbf{K}_{\mathrm{b},\mathrm{v}_n} \\ \vdots & \vdots & \ddots & \vdots & \vdots & \vdots & \vdots & \vdots \\ \mathbf{0} & \mathbf{0} & \cdots & \boldsymbol{\Theta}_{\mathrm{K}}^m & \boldsymbol{\varphi}_m^{\mathrm{T}}\mathbf{K}_{\mathrm{b},\mathrm{v}_1} & \boldsymbol{\varphi}_m^{\mathrm{T}}\mathbf{K}_{\mathrm{b},\mathrm{v}_2} & \cdots & \boldsymbol{\varphi}_m^{\mathrm{T}}\mathbf{K}_{\mathrm{b},\mathrm{v}_n} \\ \mathbf{K}_{\mathrm{v}_1,\mathrm{b}}\boldsymbol{\varphi}_1 & \mathbf{K}_{\mathrm{v}_1,\mathrm{b}}\boldsymbol{\varphi}_2 & \cdots & \mathbf{K}_{\mathrm{v}_1,\mathrm{b}}\boldsymbol{\varphi}_m & \mathbf{C}_{\mathrm{v}_1} & \mathbf{0} & \cdots & \mathbf{0} \\ \mathbf{K}_{\mathrm{v}_2,\mathrm{b}}\boldsymbol{\varphi}_1 & \mathbf{K}_{\mathrm{v}_2,\mathrm{b}}\boldsymbol{\varphi}_2 & \cdots & \mathbf{K}_{\mathrm{v}_2,\mathrm{b}}\boldsymbol{\varphi}_m & \mathbf{0} & \mathbf{C}_{\mathrm{v}_2} & \cdots & \mathbf{0} \\ \vdots & \vdots & \vdots & \vdots & \vdots & \vdots & \ddots & \vdots \\ \mathbf{K}_{\mathrm{v}_n,\mathrm{b}}\boldsymbol{\varphi}_1 & \mathbf{K}_{\mathrm{v}_n,\mathrm{b}}\boldsymbol{\varphi}_2 & \cdots & \mathbf{K}_{\mathrm{v}_n,\mathrm{b}}\boldsymbol{\varphi}_m & \mathbf{0} & \mathbf{0} & \cdots & \mathbf{C}_{\mathrm{v}_n} \end{bmatrix} \begin{Bmatrix} \boldsymbol{\xi}_1^{\mathrm{d}} \\ \boldsymbol{\xi}_2^{\mathrm{d}} \\ \vdots \\ \boldsymbol{\xi}_m^{\mathrm{d}} \\ \mathbf{q}_1 \\ \mathbf{q}_2 \\ \vdots \\ \mathbf{q}_n \end{Bmatrix} = \begin{Bmatrix} \boldsymbol{\varphi}_1^{\mathrm{T}}\mathbf{F}_{\mathrm{bu}}^{\mathrm{eq}} + \boldsymbol{\varphi}_1^{\mathrm{T}}\sum_{i=1}^{n}\mathbf{F}_{\mathrm{v}_i}{}^{\mathrm{G}} + \boldsymbol{\varphi}_1^{\mathrm{T}}\mathbf{F}_{\mathrm{b}}^{\mathrm{r}} \\ \boldsymbol{\varphi}_2^{\mathrm{T}}\mathbf{F}_{\mathrm{bu}}^{\mathrm{eq}} + \boldsymbol{\varphi}_2^{\mathrm{T}}\sum_{i=1}^{n}\mathbf{F}_{\mathrm{v}_i}{}^{\mathrm{G}} + \boldsymbol{\varphi}_2^{\mathrm{T}}\mathbf{F}_{\mathrm{b}}^{\mathrm{r}} \\ \vdots \\ \boldsymbol{\varphi}_m^{\mathrm{T}}\mathbf{F}_{\mathrm{bu}}^{\mathrm{eq}} + \boldsymbol{\varphi}_m^{\mathrm{T}}\sum_{i=1}^{n}\mathbf{F}_{\mathrm{v}_i}{}^{\mathrm{G}} + \boldsymbol{\varphi}_m^{\mathrm{T}}\mathbf{F}_{\mathrm{b}}^{\mathrm{r}} \\ \mathbf{F}_{\mathrm{v}_1}^{\mathrm{eq}} + \mathbf{F}_{\mathrm{v}_1}{}^{\mathrm{r}} \\ \mathbf{F}_{\mathrm{v}_2}^{\mathrm{eq}} + \mathbf{F}_{\mathrm{v}_2}{}^{\mathrm{r}} \\ \vdots \\ \mathbf{F}_{\mathrm{v}_n}^{\mathrm{eq}} + \mathbf{F}_{\mathrm{v}_n}{}^{\mathrm{r}} \end{Bmatrix}$$

(Eq. 30)

in which, $\boldsymbol{\Theta}_{\mathrm{C}}^{\mathrm{j}} = 2\omega_j\eta_j\boldsymbol{\varphi}_{\mathrm{j}}^{\mathrm{T}}\mathbf{M}_{\mathrm{bu}}\boldsymbol{\varphi}_{\mathrm{j}} + \boldsymbol{\varphi}_{\mathrm{j}}^{\mathrm{T}}\sum_{\mathrm{i}=1}^{\mathrm{n}}\mathbf{C}_{\mathrm{bci}}\boldsymbol{\varphi}_{\mathrm{j}}$ $j = 1,2,...,m$; $\boldsymbol{\Theta}_{\mathrm{K}}^{\mathrm{j}} = \omega_j^2\boldsymbol{\varphi}_{\mathrm{j}}^{\mathrm{T}}\mathbf{M}_{\mathrm{bu}}\boldsymbol{\varphi}_{\mathrm{j}} + \boldsymbol{\varphi}_{\mathrm{j}}^{\mathrm{T}}\sum_{\mathrm{i}=1}^{\mathrm{n}}\mathbf{C}_{\mathrm{bci}}\boldsymbol{\varphi}_{\mathrm{j}}$ $j = 1,2,...,m$

The equations of motion are solved through the Newmark-Beta method with average acceleration, and responses corresponding to generalized coordinates are obtained. The bridge dynamic responses corresponding to physical coordinates can be obtained through multiplication of the modal matrix and generalized coordinates, as shown in Eq. (27). The bridge pseudo-static response can be obtained through the influence matrix and earthquake ground motion displacements in Eq. (19). The bridge total response can be obtained by summing the dynamic response and pseudo-static response as shown in Eq. (16), while the vehicle total response is equal to the vehicle dynamic response from the coupled seismic analysis in the bridge-traffic system.

4. NUMERICAL SIMULATION RESULTS

4.1 Prototype Bridge and Traffic System

The prototype long-span bridge in this study has a total length of 840 m, including a main span, two side spans and two approach spans, as shown in Figure 4.1. The cable-stayed bridge has a bridge deck with a constant steel twin-box cross-section that has a width of 28 m and a height of 4.57 m. The two steel pylons have A-shaped cross-sections with a height of 103.6 m. The bridge superstructure is supported by the reinforced concrete bridge piers with sliding bearings at the side span. The two fan-shaped cable planes of the bridge have 12 sparsely located cables in each cable plane. The six support locations are labeled as support 1 to 6 in Figure 4.1 for spatially varying ground motion inputs.

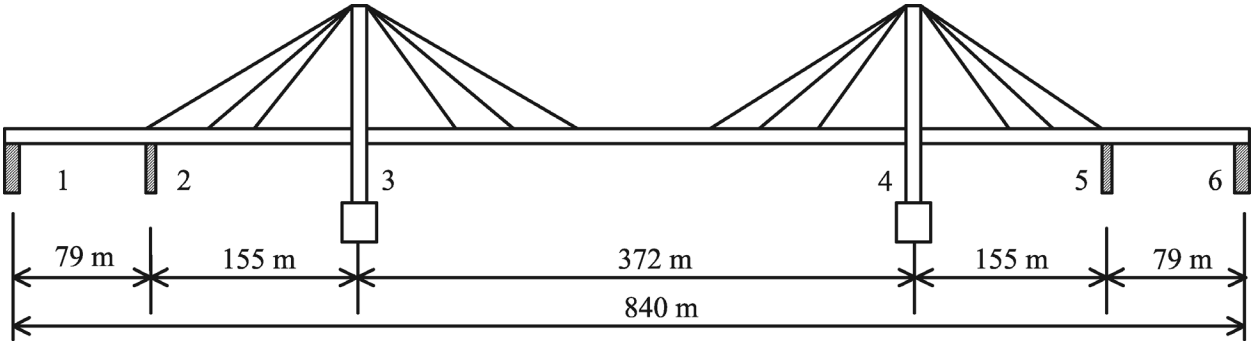

Figure 4.1 Elevation view of the prototype bridge

The bridge is modeled using three elements: Timoshenko beam, catenary cable and link. The bridge girders, piers and pylons are modeled using Timoshenko beam elements. The stay cables are modeled using catenary cable elements. The deck is connected to the tower cross beam using rigid link elements with zero mass, which are fixed in each of the six DOFs, including three translational DOFs and three rotational DOFs. The deck is connected to piers through sliding bearings. The sliding bearing allows energy dissipation in the longitudinal direction and is modeled as a nonlinear link element with zero mass, of which all the other DOFs are fixed except the translational DOF in the longitudinal direction. The piers and pylons are assumed to be fixed on the ground without considering soil-structure interactions. The mass density of structural steel and concrete is 74.87 kN/m^3 and 23.56 kN/m^3, respectively. The elastic modulus of structural steel and concrete is 1.999×10^8 kN/m^2 and 2.779×10^7 kN/m^2, respectively. Poisson's ratio of structural steel and concrete is 0.27 and 0.20, respectively. Rayleigh damping model is used in the study to consider damping effects, in which the participating factor for stiffness and mass matrix are obtained from the first two bending modes by assuming a damping ratio of 0.01.

Frequencies and mode shape features of the bridge structure are determined by means of the eigenvalue analysis on the finite element model of the bridge. The first 12 modes including modal frequencies and dominant mode shapes on the bridge girder are given in Table 4.1. It is found from the preliminary sensitivity analysis that the first several modes dominate the vibration properties of the bridge and the bridge response exhibits little change when the number of involved modes is beyond 60. Therefore, the first 60 modes of the bridge are adopted in this study to establish equations of motion of the bridge-traffic system under seismic excitations.

Table 4.1 Modal properties of the first 12 modes of the prototype bridge

Mode number	Mode frequency (Hz)	Dominating mode shape
1	0.42	1st vertical
2	0.46	1st lateral
3	0.56	2nd lateral
4	0.63	1st longitudinal; 2nd vertical
5	0.65	3rd lateral
6	0.79	2nd longitudinal; 3rd vertical
7	1.01	4th vertical
8	1.07	Tower mode
9	1.09	Tower mode
10	1.11	5th vertical
11	1.20	1st torsional
12	1.23	6th vertical

The traffic flow pattern is assumed to have a moderate density of 20 vehicles/km/lane, which is simulated in two lanes in each of the two driving directions. Percentages of the three types of vehicles in the traffic flow are assumed to be 20%, 30%, and 50% for heavy trucks, light trucks, and light cars, respectively, representing a typical vehicle composition in the traffic flow. The roadway-bridge-roadway route contains 112 cells for the bridge path and 28 cells for each of the two roadway paths with a cell length of 7.5 m. Total length of the roadway-bridge-roadway path is 1260 m, including two roadways with a length of 210 m each and the bridge with a length of 840 m. The simulated stochastic traffic flow at a moderate traffic density consists of 108 vehicles on the roadway-bridge-roadway system, including 20 heavy trucks, 32 light trucks, and 56 light cars. The number of DOFs of the bridge-traffic system is 1,536, in which the first 60 DOFs are in the modal coordinates of the bridge corresponding to the first 60 modes and the later 1,436 DOFs are in the physical coordinates for all the vehicles. The busy traffic flow is simulated stochastically with time duration of 50 seconds.

Figure 4.2 shows the longitudinal locations of the vehicles with respect to time on one lane of the bridge in the traffic flow. Unlike the bridge structure, in which modal coordinates are involved in the equations of motion, the physical coordinates of the vehicles are directly used in the equations of motion. For better understanding of the vibration properties of the vehicles, eigenvalue analysis is also conducted on each type of the vehicles to obtain modal frequencies and mode shapes. The heavy truck model has 19 DOFs and therefore, 19 modes. The light truck and light car model has 12 modes corresponding to the 12 DOFs. The mode frequencies and dominating DOFs in the first eight modes of the heavy truck model and the first six modes of the light truck and light car model are given in Table 4.2. The dynamic properties, including mass, mass moment of inertia, stiffness coefficients, and damping coefficients, and the dimension parameters of the heavy truck, light truck, and light car model can be found in Zhou and Chen (2015b).

Table 4.2 Modal properties of the heavy truck, light truck, and light car

	Mode number	Mode frequency (Hz)	Dominating DOFs
Heavy truck	1	0.554	Y_{a2R}, Y_{a3L}, Y_{a3R}
	2	0.886	Z_{r1}, θ_{r1}, Z_{r2}, θ_{r2}, Z_{a1L}, Z_{a1R}, Z_{a2L}
	3	0.980	Y_{r1}, Y_{r2}, Y_{a1L}, Y_{a1R}, Y_{a2L}
	4	1.009	θ_{r1}, Z_{r2}, β_{r2}, Z_{a1L}, Z_{a1R}, Z_{a2L}
	5	1.104	Z_{a2R}, Z_{a3L}, Z_{a3R}
	6	1.682	Z_{r1}, θ_{r1}, Z_{a1L}, Z_{a1R}, Z_{a2L}, Z_{a3L}, Z_{a3R}
	7	1.836	β_{r1}, Z_{a1L}, Z_{a1R}, Z_{a2L}, Z_{a2R}
	8	2.541	Y_{a1R}, Y_{a2L}
Light truck	1	1.107	Z_{a1L}, Z_{a1R}, Z_{a2L}, Z_{a2R}
	2	1.196	Y_{r1}, Y_{a1L}, Y_{a1R}, Y_{a2L}, Y_{a2R}
	3	1.513	β_{r1}, Z_{a1L}, Z_{a1R}, Z_{a2L}, Z_{a2R}
	4	2.100	θ_{r1}, Z_{a1L}, Z_{a1R}, Z_{a2L}, Z_{a2R}
	5	3.632	Z_{a1L}, Z_{a1R}, Z_{a2L}, Z_{a2R}
	6	3.948	Z_{r1}, Z_{a1L}, Z_{a1R}, Z_{a2L}, Z_{a2R}
Light car	1	0.826	Y_{r1}, Y_{a1L}, Y_{a1R}, Y_{a2L}, Y_{a2R}
	2	1.138	Z_{r1}, θ_{r1}, Z_{a1L}, Z_{a1R}, Z_{a2L}, Z_{a2R}
	3	1.351	Z_{r1}, θ_{r1}, Z_{a1L}, Z_{a1R}, Z_{a2L}, Z_{a2R}
	4	1.517	β_{r1}, Z_{a1L}, Z_{a1R}, Z_{a2L}, Z_{a2R}
	5	3.972	Y_{a1L}, Y_{a1R}, Y_{a2L}, Y_{a2R}
	6	4.004	Y_{a1L}, Y_{a1R}, Y_{a2L}, Y_{a2R}

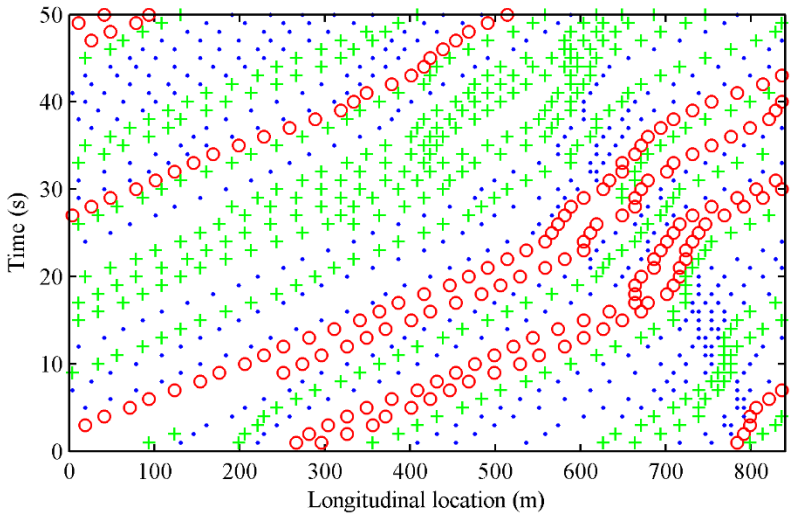

Figure 4.2 Time-varying vehicle longitudinal locations on the bridge in one traffic lane (o - heavy truck; + - light truck; · - light car)

4.2 Spatially Varying Earthquake Excitations

To demonstrate the proposed methodology, one set of earthquake records from the Imperial Earthquake is selected as the scenario earthquake for demonstration purposes. The Imperial Earthquake record in the present study has a time step of 0.02 s, which is shorter than the required time step of 0.04 s under moving traffic. Therefore, the integration time step for the equations of motion of the bridge-traffic system under earthquake is set to be 0.02 s in the present study. The horizontal component of the example seismic shear wave is shown in Figure 4.3. The attack angle of the seismic wave is assumed to be 45° to the longitudinal axis of the bridge structure. The vertical to horizontal ratio of the earthquake is selected as 2/3 based on some existing regulations to incorporate the vertical earthquake ground motion excitations (ASCE 2010). Through the STFT, the evolutionary PSDF is obtained with respect to time and frequency, which is demonstrated in Figure 4.4. It can be seen in Figure 4.4 that energy content of the example earthquake record is concentrated in the frequency range from 0–20 Hz and the time range from 2–30 s.

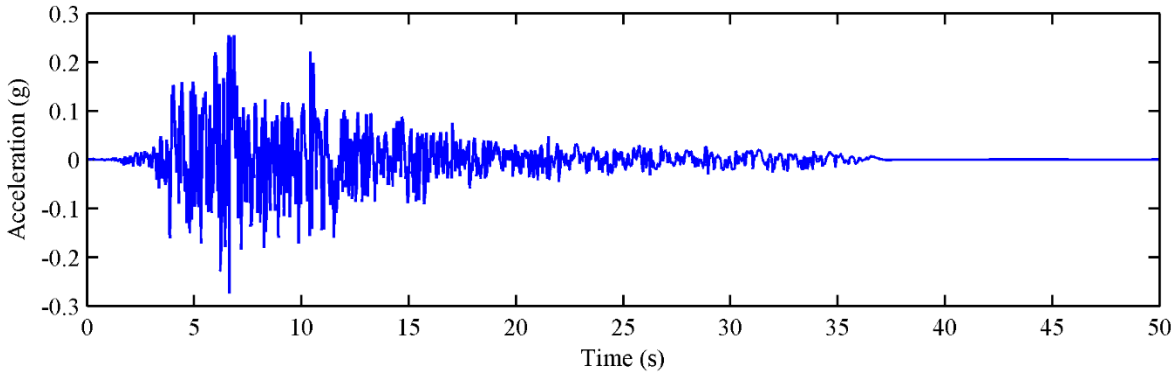

Figure 4.3 Acceleration time history of the horizontal component of a scenario earthquake record

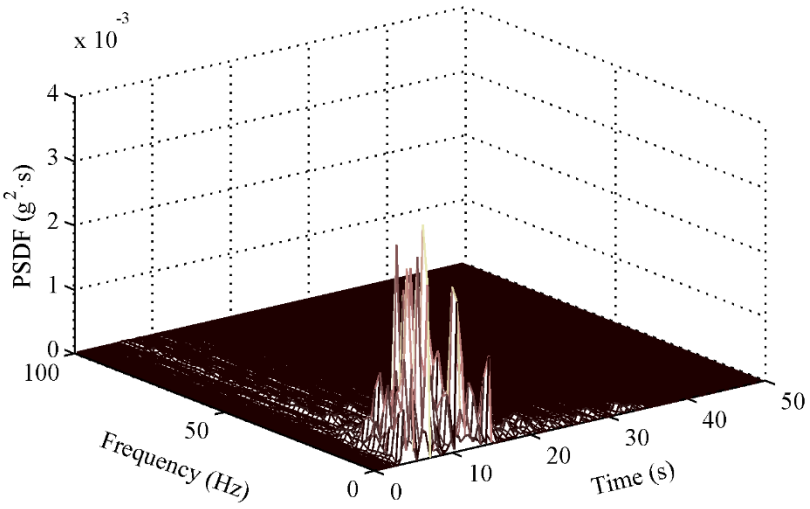

Figure 4.4 Evolutionary PSDF of the scenario earthquake record using STFT

With the spectral-representation-based simulation algorithm, six sets of synthetic ground motion acceleration time histories are generated as non-stationary stochastic processes for the six different support locations. The spatial variability due to the incoherence effect, wave-passage effect and site response effect has been taken into account. The acceleration time histories at supports 1, 3, and 5 are demonstrated in Figure 4.5a, b and c, respectively. Through the post-processing techniques including Butterworth filtering and baseline correction, the velocity and displacement time histories for each

acceleration input at the supports are obtained. The velocity time histories of the earthquake ground motions for supports 1, 3, and 5 are demonstrated in Figure 4.5. The velocity and displacement time histories of the earthquake ground motions for supports 1, 3, and 5 are demonstrated in Figures 4.6 and 4.7, respectively. The velocity time histories have zero values at the end after baseline correction. The displacement time histories have a very small offset from zero at the end due to the remaining numerical error during baseline correction.

As shown in Figures 4.5, 4.6, and 4.7, the velocity and displacement time histories of earthquake ground motions have very different frequency components from those of the acceleration histories. For earthquake acceleration time histories, it is a broad-band random process. Comparatively, earthquake velocity and displacement time histories have very low frequency contents (lowest for the earthquake displacement). The difference of the phase angle for the acceleration histories at different supports can also be reflected in the velocity and displacement histories at different supports. For instance, significant phase lag is observed in the earthquake displacement time history at support 5, as compared to that at support 1.

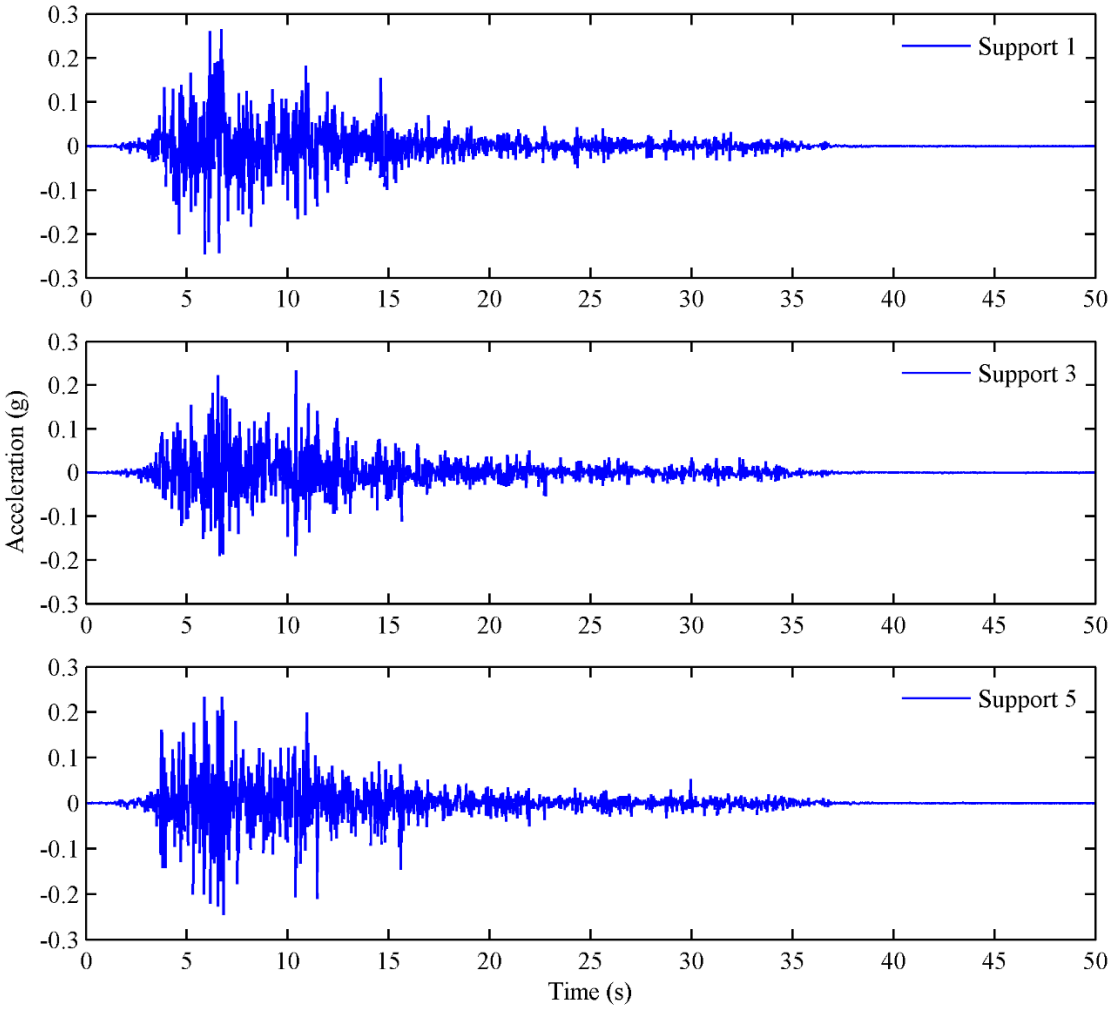

Figure 4.5 Simulated ground motion acceleration at support locations 1, 3 and 5

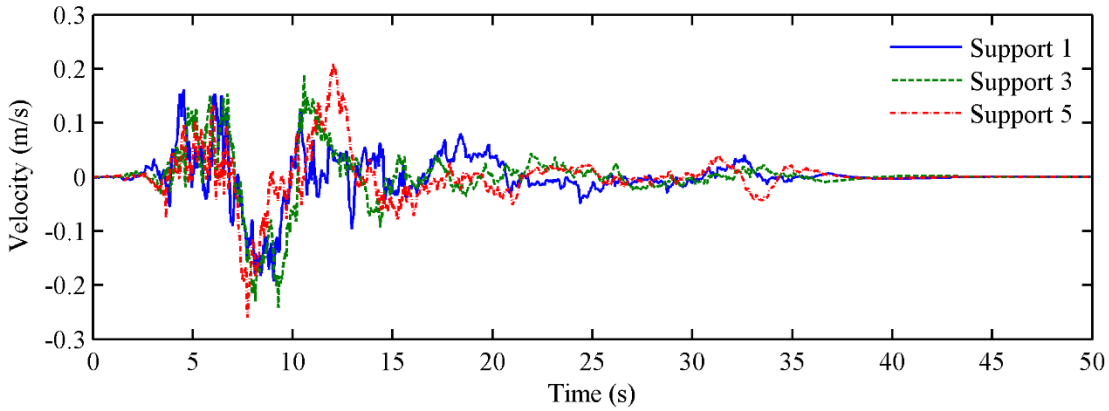

Figure 4.6 Simulated ground motion velocity at support locations 1, 3 and 5

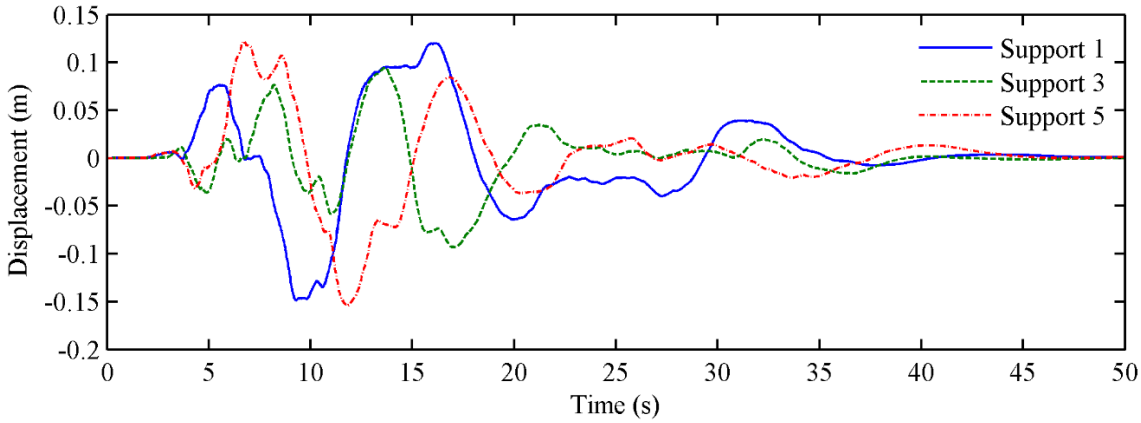

Figure 4.7 Simulated ground motion displacement at support locations 1, 3 and 5

4.3 Full-response Assessment of Bridge for Baseline Scenario

For the baseline scenario, spatially varying earthquake ground motions are applied at the bridge supports when moderate traffic flow is present on the bridge. Coupled seismic analysis is conducted on the bridge-traffic system with the time duration of 50 seconds to obtain the dynamic response of the bridge and individual vehicles in the traffic flow. The pseudo-static response of the bridge is obtained through the multiplication of influence matrix and support ground motion displacement vector. The total bridge response is obtained by summing the dynamic response and pseudo-static response at each time step. The vertical, lateral, and longitudinal displacement time histories at the bridge mid-span are shown in Figure 4.8a, b, and c, respectively.

In each subplot of Figure 4.8, the total, dynamic and pseudo-static displacement time histories are plotted together for comparison. It can be seen that the bridge vibrates at frequencies of their fundamental modes for vertical, lateral, and longitudinal directions. Taking the vertical displacement as an example, the fundamental vertical frequency is 0.42 Hz which is the dominant vibrating frequency of the vertical dynamic and total responses. The pseudo-static response has very low vibrating frequencies in each vibrating direction, which are much lower than natural frequencies of the bridge structure. For the vertical response, the dynamic response is dominant in the total bridge response. However, for lateral and longitudinal displacement responses, the extreme responses are dominated by the pseudo-static response. Considering that the bridge-traffic interaction is much stronger in the vertical direction than those in lateral and longitudinal directions, dynamic response in the vertical direction accounts for a much larger proportion in the total response than those in the other two directions.

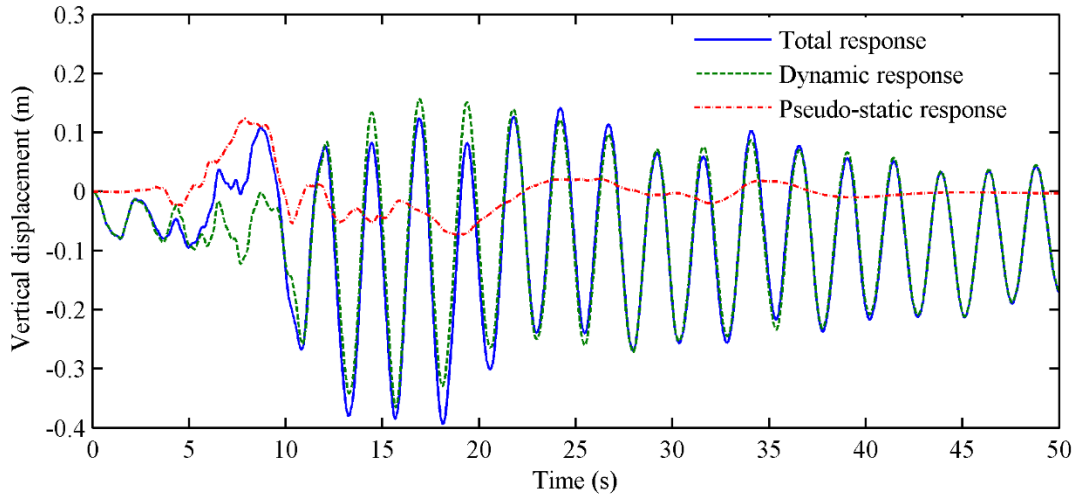

(a) Vertical displacement

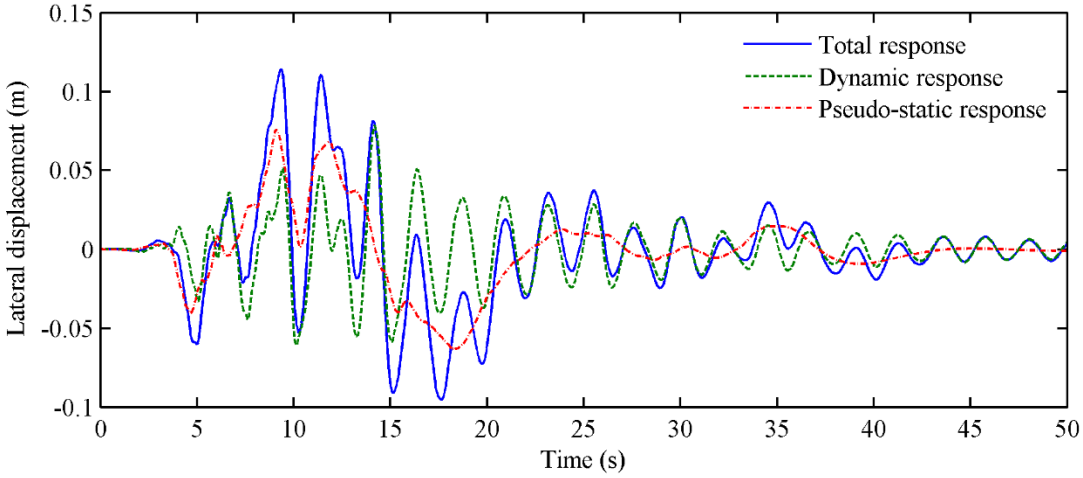

(b) Lateral displacement

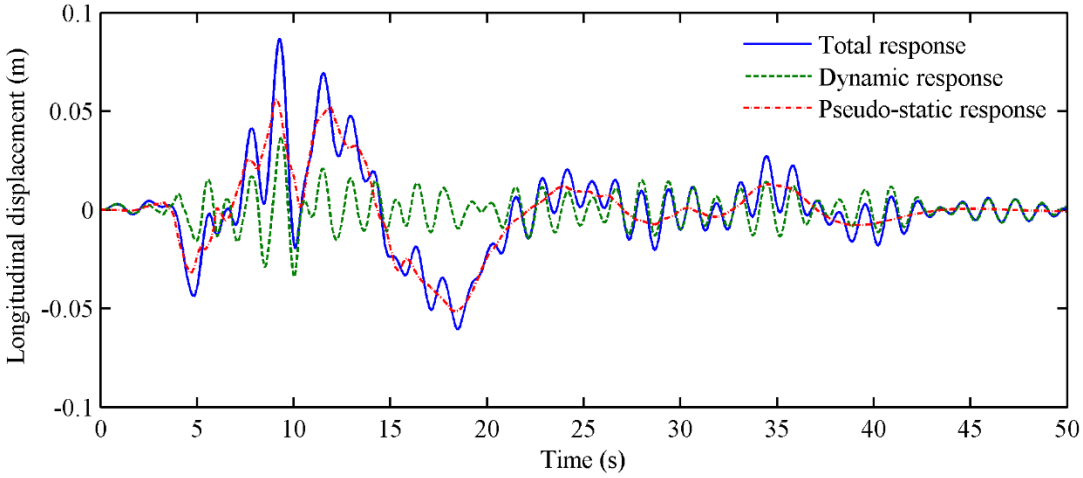

(c) Longitudinal displacement

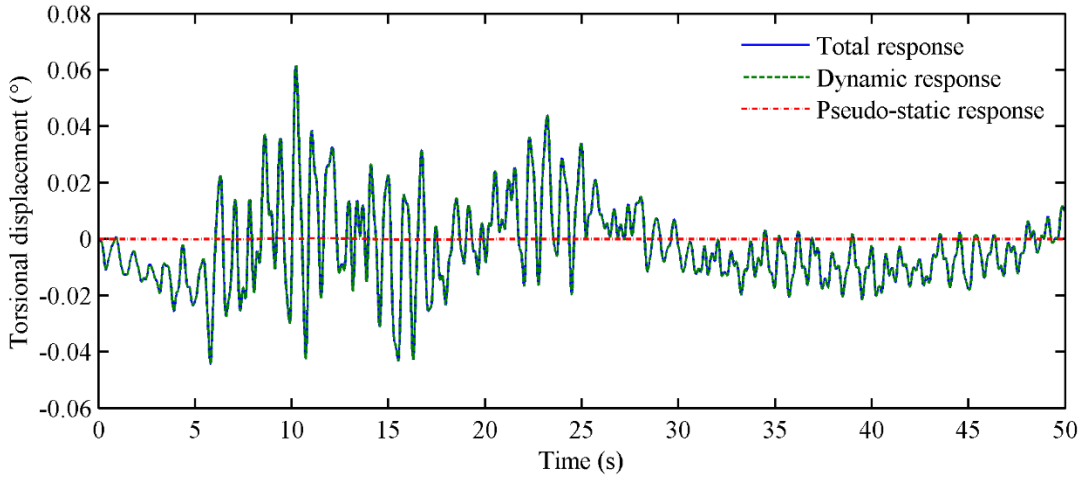

(d) Torsional displacement

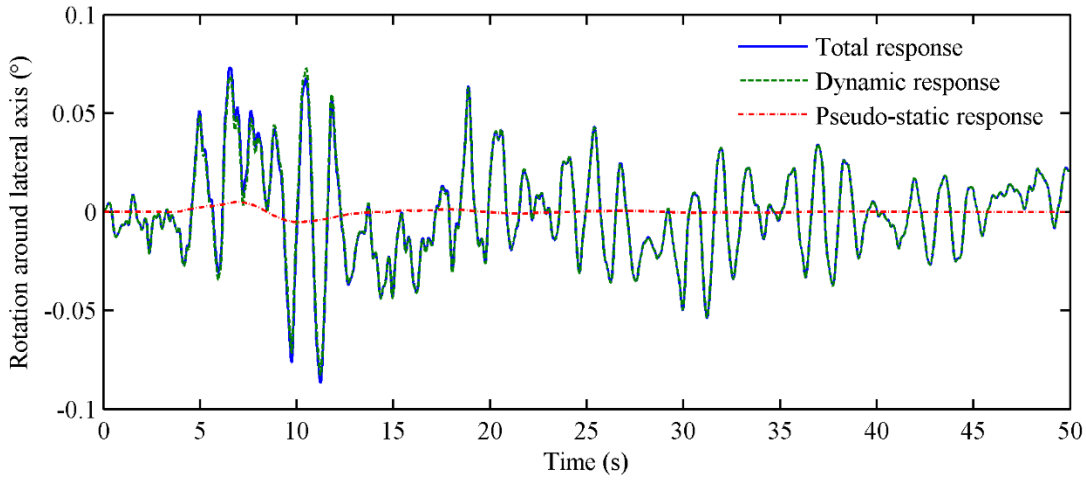

(e) Rotational displacement around lateral axis

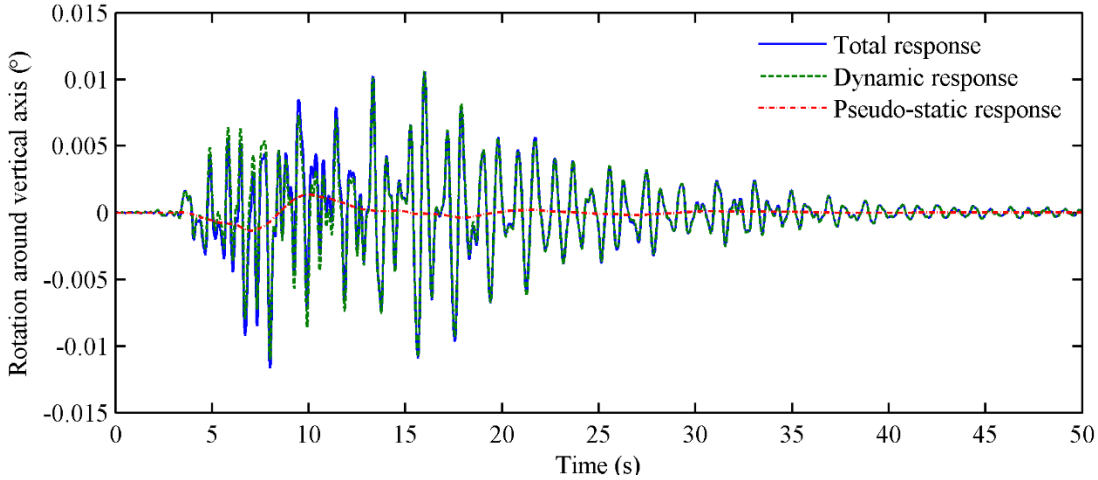

(f) Rotational displacement around vertical axis

Figure 4.8 Full response results of the bridge in the three translational directions in the baseline scenario

The displacement time histories in the three rotational directions around longitudinal, lateral and vertical axes are plotted in Figure 4.8d, e, and f, respectively. Rotational displacement around longitudinal axis is also noted as torsional displacement. The bridge pseudo-static responses in the rotational direction are much less significant than those in translational directions. Apparently, dynamic response is the dominant part of the total bridge response in rotational directions.

4.4 Impact of Moving Traffic on Bridge Seismic Response

The influence of moving traffic on the bridge structure under seismic excitations is investigated in this section. Three loading scenarios were conducted, and response results were compared. In the first scenario, earthquake excitations were applied at the bridge supports when vehicles in a moderate traffic flow travel through the bridge. In the second scenario, the bridge vibrated only under the excitations from earthquake and the moving vehicles were not involved. In the third scenario, the bridge vibrated under moving vehicles in the moderate traffic flow without considering earthquake excitations. The vertical, lateral, and torsional displacements at the bridge mid-span in the three comparative scenarios are demonstrated in Figure 4.9a, b and c, respectively. The largest extreme vertical, lateral, and torsional responses occur when earthquake excitations and stochastic traffic are considered simultaneously. Under only the excitations from the traffic flow, the bridge had little lateral displacement but had significant responses for vertical and torsional dynamic displacements. The vertical, lateral, and torsional displacements of the bridge under only seismic excitations have mean values close to zero. Comparatively, the bridge vertical displacement under only traffic flow excitations had a non-zero mean value, which is mainly due to the gravity forces of moving vehicles through the bridge. The mean value of the bridge torsional displacement varied from time to time during the simulation period since the locations of moving vehicles vary notably, which caused unsymmetrical torsional displacement of the bridge. However, the mean value of the bridge torsional displacement will approach zero if the mean value is obtained through a sufficiently long simulation period.

Figure 4.9a, b and c show that variation of the displacement response in one response cycle is much larger in the scenario with only earthquake excitations than in the scenario with only traffic flow excitations. This implies that larger dynamic effects are induced on the bridge structure by the earthquake excitations than those from stochastic traffic flow. For a linear system, linear superposition usually stands when considering multiple excitations. In other words, the response of a linear system under multiple excitations should be equal to the summation of the response under each of the several excitations. Bridge displacement under simultaneous excitations from earthquake and traffic flow is much larger than summation of the individual displacements under only earthquake and under only traffic flow in each direction. This indicates that significant nonlinearities are involved in the interaction effects in the coupled bridge-traffic system under seismic excitations, especially in the vertical direction, at which the interaction effects between the bridge and vehicles are most significant.

It again confirms that simple linear superposition of the results from traditional analyses of individual loads (e.g., earthquake and traffic) is not appropriate. Results clearly show that the proposed methodology can take into account various coupling effects, not only between the bridge and moving traffic, but also between earthquake forces and bridge-traffic interaction system. Therefore, the proposed methodology for the first time offers a simulation tool to predict the full response of the bridge and moving highway traffic under spatially-varying seismic excitations by considering various coupling effects.

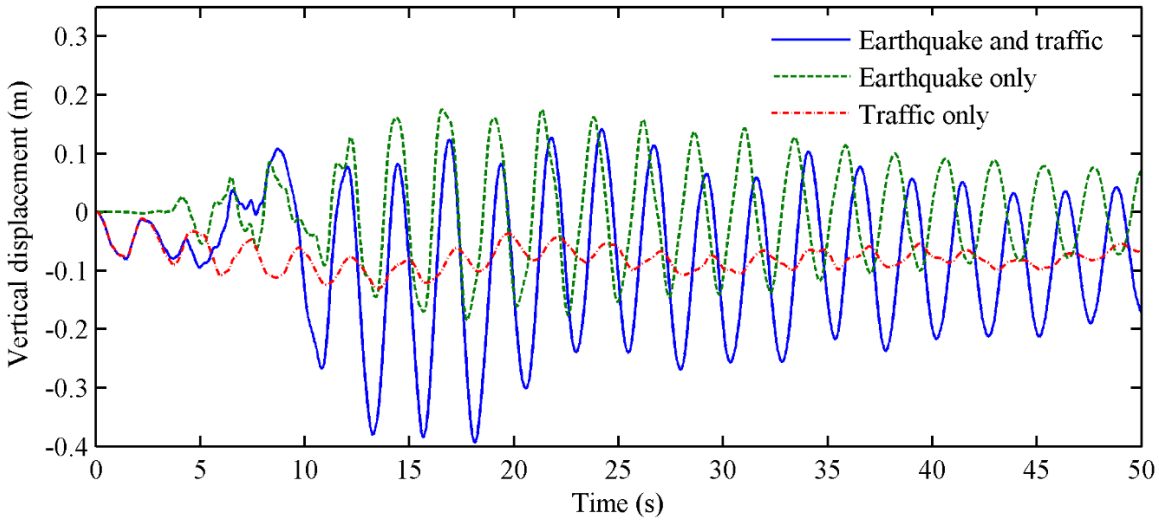

(a) Vertical displacement

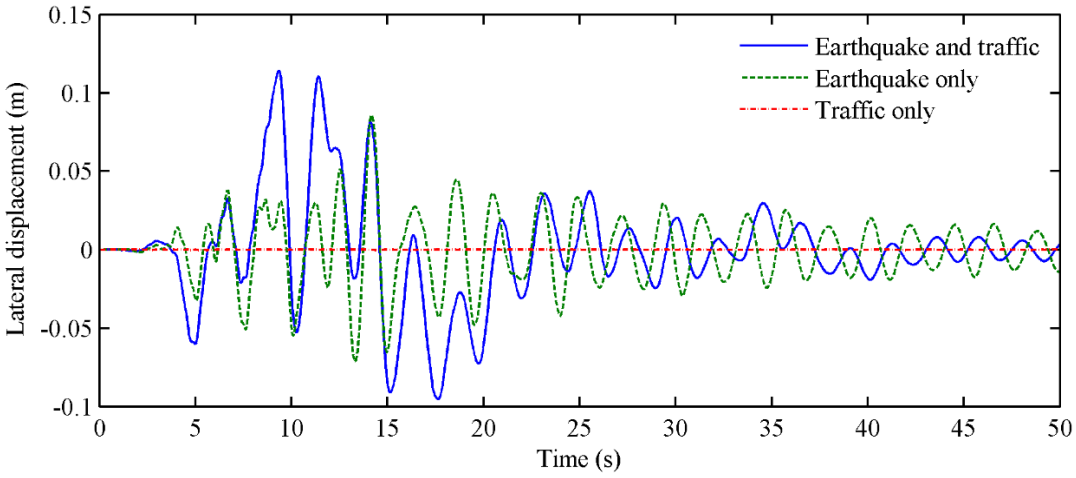

(b) Lateral displacement

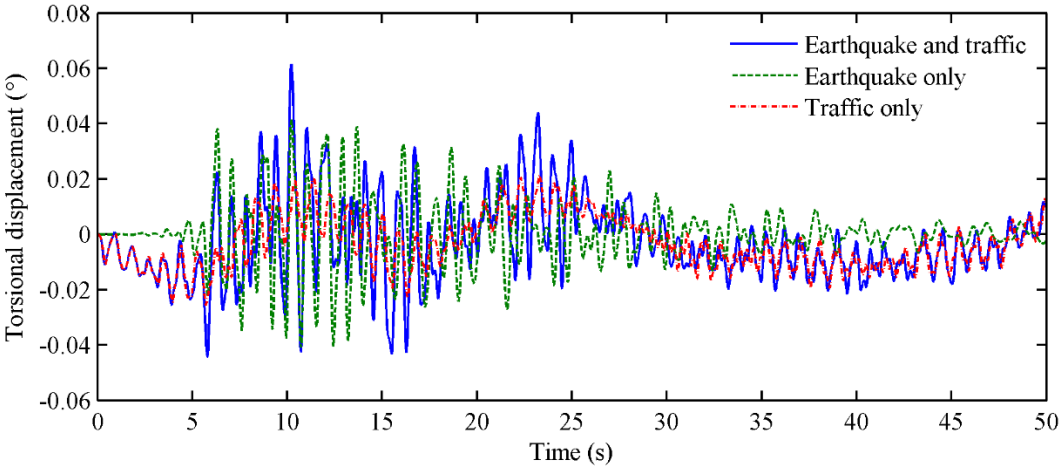

(c) Torsional displacement

Figure 4.9 Comparison of bridge response under different combinations of earthquake and traffic

4.5 Impact of Coupling Earthquake Forces on Dynamic Response of Bridge-traffic System

By taking into account the coupled earthquake forces in addition to traditional earthquake forces, the coupling effects in the bridge-traffic system under seismic excitations can be more comprehensively considered and dynamic performance of the bridge-traffic system can be more accurately predicted. In this section, the influence of the coupling earthquake forces on the dynamic response of the bridge-traffic system will be studied by comparing responses of the bridge and moving vehicles in two comparative cases. In the first case, the dynamic analysis is conducted on the bridge-traffic system under seismic excitations considering traditional and coupling earthquake forces using the proposed methodology in the present study. In the second case, the dynamic analysis is conducted on the same bridge-traffic system under the same set of spatially varying earthquake excitations considering only the traditional earthquake forces. The responses and forces acting on the bridge and the representative vehicle are investigated in the two comparative cases that follow.

4.5.1 Bridge Response

Since the pseudo-static responses for the bridge are the same in the two cases, only the bridge dynamic responses are shown and compared to demonstrate differences in responses of the two cases. Figure 4.10a, b, and c show the vertical, lateral, and rotational displacements at the bridge mid-span, respectively. Figure 4.10 shows that larger extreme responses in each direction occur when coupled earthquake forces are considered in addition to traditional earthquake forces. It implies that by taking into account the coupling effects between the bridge-traffic system and earthquake forces, the bridge structure has a higher risk of exceeding serviceability or strength thresholds. Although not displayed for the concise purpose, the displacement responses in the other three directions at the bridge mid-span also induce larger extreme responses in the case with coupled and traditional earthquake forces than those in the case with only traditional earthquake forces. The absolute extreme responses of the vertical, lateral, and torsional displacements considering coupled and traditional earthquake forces are 0.37 m, 0.078 m, and 0.073°, respectively.

In contrast, the absolute extreme responses of the vertical, lateral and rotational displacements considering only traditional earthquake forces are 0.31 m, 0.074 m, and 0.061°, respectively. By considering the coupled earthquake forces in addition to the traditional earthquake forces, the extreme responses are increased by 19%, 5%, and 20 %, respectively. The coupling effects between the earthquake forces and the bridge-traffic interaction system are stronger in the vertical and torsional directions than those in the lateral direction. The finding can be explained from the nature of the dynamic interaction between the bridge and vehicles. The vertical interactions between the bridge and vehicles are determined from the relative vertical displacements between the bridge and vehicle wheels at contact point. The relative vertical displacements at bridge-wheel contact point are obtained from the vertical and torsional displacements at the torsional center of the bridge section, as indicated in Eq. (10). Since the interaction effects between the bridge and vehicles are stronger in the vertical direction than in the lateral direction, the vertical and torsional displacements of the bridge structure are more likely to be influenced in the bridge-traffic interaction system. When earthquake excitations are also involved, the coupling effects between the earthquake forces and bridge-traffic interaction tend to be more remarkable in the directions with stronger bridge-traffic interactions.

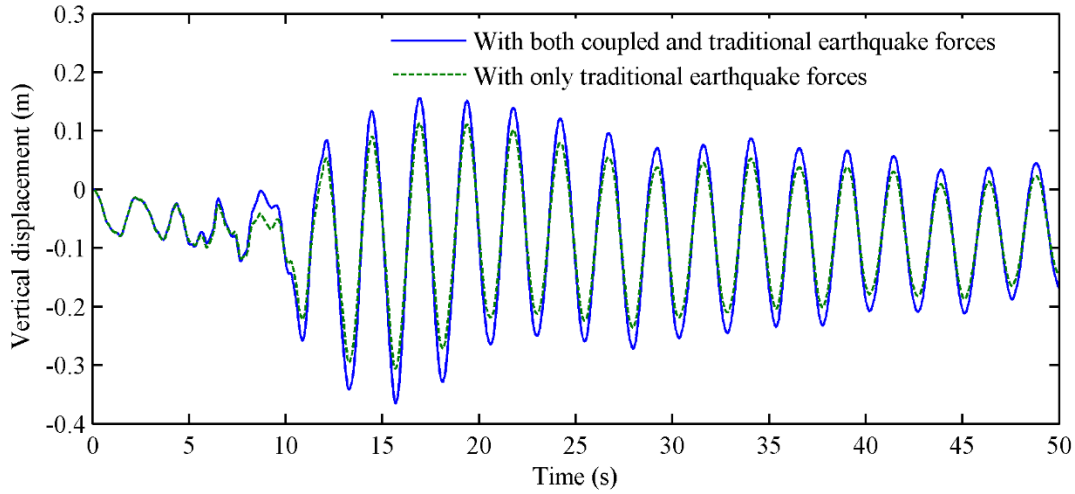

(a) Vertical displacement

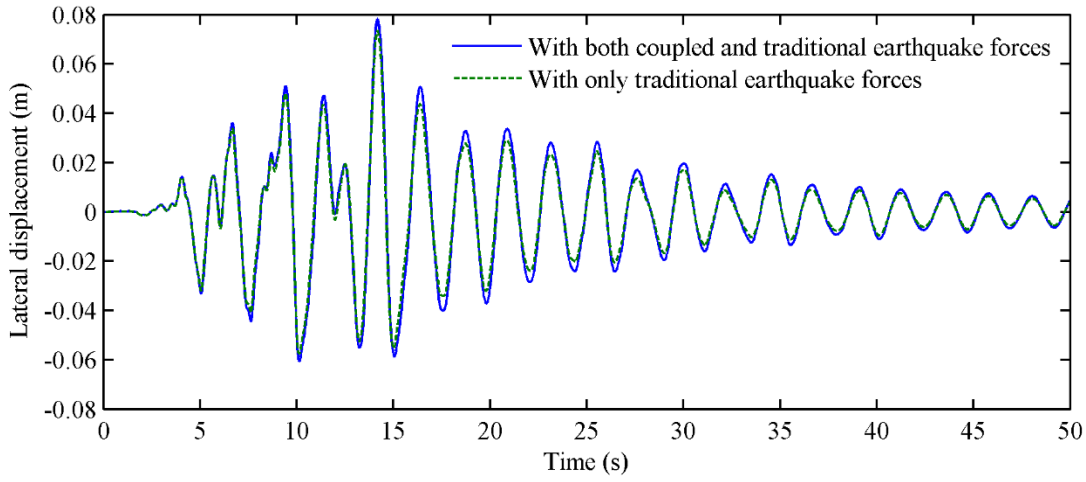

(b) Lateral displacement

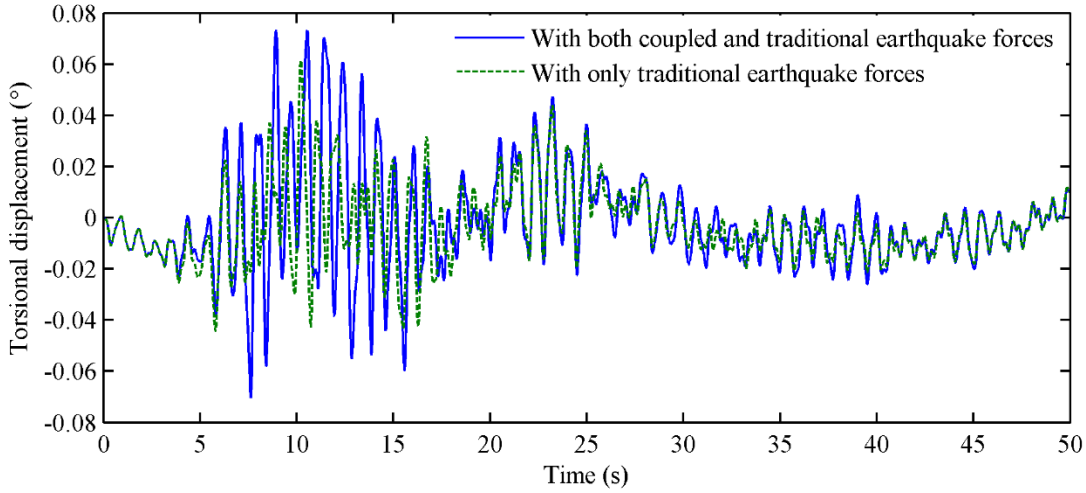

(c) Torsional displacement

Figure 4.3 Comparison of the bridge dynamic responses with or without coupled earthquake forces

In the coupled bridge-traffic system under seismic excitations, several sources of excitations contribute to responses of the bridge and moving vehicles. For the bridge structure, the sources of excitations include traditional earthquake force, coupled earthquake force and bridge-vehicle interaction force on the bridge structure. The bridge-vehicle interaction force on the bridge structure is obtained from bridge-wheel contact force due to vehicle gravity, road surface roughness, and coupling effects with the vehicles. After the vector of generalized coordinate is obtained in each time step from Eq. (30), the bridge-traffic interaction force on the bridge structure corresponding to the j^{th} mode can be formulated in the following equation.

$$\mathbf{F}_{\mathbf{j}}^{\mathbf{b-v}} = \boldsymbol{\varphi}_{\mathbf{j}}^{\mathbf{T}} \sum_{\mathbf{i=1}}^{\mathbf{n}} \mathbf{F}_{\mathbf{v_i}}^{\mathbf{G}} + \boldsymbol{\varphi}_{\mathbf{j}}^{\mathbf{T}} \mathbf{F}_{\mathbf{b}}^{\mathbf{r}} - \boldsymbol{\varphi}_{\mathbf{j}}^{\mathbf{T}} \sum_{\mathbf{i=1}}^{\mathbf{n}} \mathbf{K}_{\mathbf{bci}} \boldsymbol{\varphi}_{\mathbf{j}} \boldsymbol{\xi}_{\mathbf{j}} - \boldsymbol{\varphi}_{\mathbf{j}}^{\mathbf{T}} \sum_{\mathbf{i=1}}^{\mathbf{n}} \mathbf{C}_{\mathbf{bci}} \boldsymbol{\varphi}_{\mathbf{j}} \dot{\boldsymbol{\xi}}_{\mathbf{j}} - \boldsymbol{\varphi}_{\mathbf{j}}^{\mathbf{T}} \sum_{\mathbf{i=1}}^{\mathbf{n}} \mathbf{K}_{\mathbf{b,v_i}} \mathbf{q}_{\mathbf{i}} - \boldsymbol{\varphi}_{\mathbf{j}}^{\mathbf{T}} \sum_{\mathbf{i=1}}^{\mathbf{n}} \mathbf{C}_{\mathbf{b,v_i}} \dot{\mathbf{q}}_{\mathbf{i}} \qquad \text{(Eq. 31)}$$

in which, F_j^{b-v} is the bridge-traffic interaction force; the superscript j means the force is corresponding to the j^{th} mode and j^{th} generalized coordinate; the first term on the right-hand side is the generalized force from vehicle gravity force; the second term on the right-hand side is the generalized force from road surface roughness; the other terms on the right-hand side are the coupling forces dependent on the bridge or vehicle motions; the term $-\boldsymbol{\varphi}_{\mathbf{j}}^{\mathbf{T}} \sum_{\mathbf{i=1}}^{\mathbf{n}} \mathbf{K}_{\mathbf{bci}} \boldsymbol{\varphi}_{\mathbf{j}} \boldsymbol{\xi}_{\mathbf{b}} - \boldsymbol{\varphi}_{\mathbf{j}}^{\mathbf{T}} \sum_{\mathbf{i=1}}^{\mathbf{n}} \mathbf{C}_{\mathbf{bci}} \boldsymbol{\varphi}_{\mathbf{j}} \dot{\boldsymbol{\xi}}_{\mathbf{b}}$ is about bridge-vehicle coupling forces acting on the bridge structure due to the bridge motion. The term $-\boldsymbol{\varphi}_{\mathbf{j}}^{\mathbf{T}} \sum_{\mathbf{i=1}}^{\mathbf{n}} \mathbf{K}_{\mathbf{b,v_i}} \mathbf{q}_{\mathbf{i}} - \boldsymbol{\varphi}_{\mathbf{j}}^{\mathbf{T}} \sum_{\mathbf{i=1}}^{\mathbf{n}} \mathbf{C}_{\mathbf{b,v_i}} \dot{\mathbf{q}}_{\mathbf{i}}$ is about the bridge-vehicle coupling forces acting on the bridge structure due to the motion of each individual vehicle in the traffic flow; n is the number of total vehicles in the traffic flow; m is the number of selected modes involved in the dynamic analysis.

The traditional and coupled earthquake forces on the bridge structure corresponding to the j^{th} mode can be expressed in the following equations, respectively:

$$\mathbf{F}_{\mathbf{bu,j}}^{\mathbf{eq,t}} = -\boldsymbol{\varphi}_{\mathbf{j}}^{\mathbf{T}} \mathbf{M}_{\mathbf{bu}} \mathbf{R} \ddot{\mathbf{u}} - \boldsymbol{\varphi}_{\mathbf{j}}^{\mathbf{T}} 2\omega_j \eta_j \mathbf{M}_{\mathbf{bu}} \mathbf{R} \dot{\mathbf{u}} \qquad \text{(Eq. 32a)}$$

$$\mathbf{F}_{\mathbf{bu,j}}^{\mathbf{eq,c}} = -\boldsymbol{\varphi}_{\mathbf{j}}^{\mathbf{T}} \sum_{\mathbf{i=1}}^{\mathbf{n}} \mathbf{C}_{\mathbf{bci}} \mathbf{R} \dot{\mathbf{u}} - \boldsymbol{\varphi}_{\mathbf{j}}^{\mathbf{T}} \sum_{\mathbf{i=1}}^{\mathbf{n}} \mathbf{K}_{\mathbf{bci}} \mathbf{R} \mathbf{u} \qquad \text{(Eq. 32b)}$$

The generalized forces for traditional earthquake force, coupled earthquake force and bridge-traffic interaction force in the first case — considering traditional and coupled earthquake force — are generated in each time step and plotted in Figure 4.11. In addition, the bridge-traffic interaction forces in the second case — considering only traditional earthquake force — are also plotted for comparison. Figure 4.11a, b, and c demonstrate the generalized force on the bridge structure corresponding to the 1st, 2 nd, and 11th mode, respectively. The modal frequencies for the 1st, 2 nd, and 11th modes are 0.42 Hz, 0.46 Hz, and 1.20 Hz, which are fundamental modes dominating in the vertical, lateral and torsional motions, respectively. It can be seen that for the 1st and 2nd modes corresponding to translational motion, the traditional earthquake force has the largest extreme values and dominates in the total force applied on the bridge. However, for the 11th mode corresponding to torsional motion, the bridge-traffic interaction force coupled with earthquake is dominant among all types of forces.

This is mainly because traditional earthquake force is dependent on ground motion acceleration inputs applied at the bridge supports in the translational rather than rotational directions. For the translational modes such as the 1st and 2nd modes, the bridge-traffic interaction force coupled with earthquake force is the second dominant force following the traditional earthquake force. It implies that earthquake force has a significant influence on interaction behavior of the bridge and moving vehicles. This is also reflected on the fact that bridge-traffic interaction force is larger when it is coupled with earthquake ground motions. By comparing Figure 4.11a and Figure 4.8a, it was found that coupled earthquake force has a similar

shape with the pseudo-static response of the bridge in the same motion direction. This can be explained by the formulation of coupled earthquake force on the bridge, which is composed of bridge-traffic coupling matrices and pseudo-static response of the bridge. Figure 4.11a, b, and c show that coupled earthquake force tends to have an opposite phase to the bridge-traffic interaction force coupled with earthquake. The coupled earthquake force reaches a local maximum positive value when bridge-traffic interaction force reaches a local maximum negative value and vice versa, especially for the translational modes in Figure 4.11a and b.

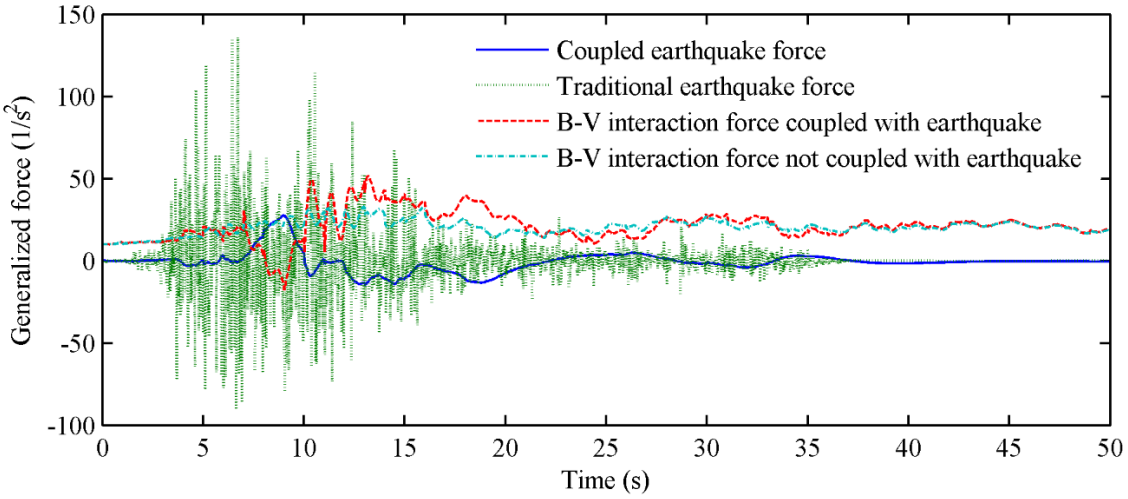

(a) The 1st mode

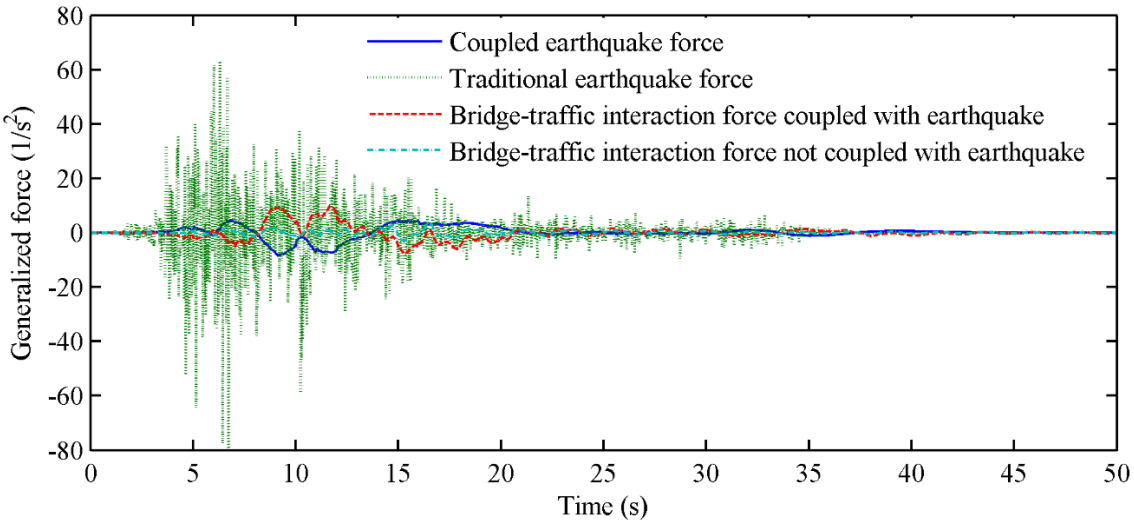

(b) The 2nd mode

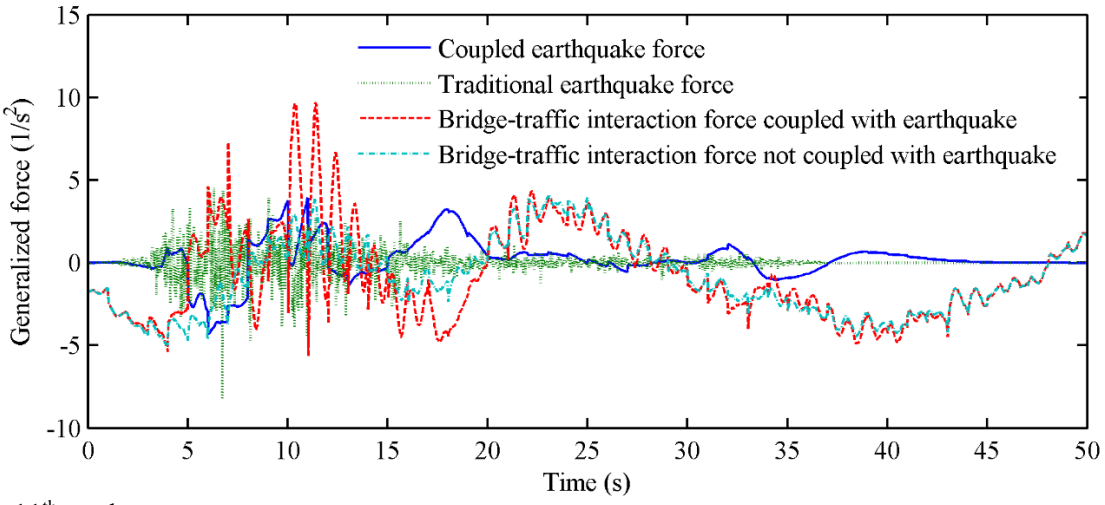

(c) The 11th mode

Figure 4.4 Generalized forces on the bridge structure corresponding to the fundamental modes

To investigate the frequency characteristics of various sources of forces have on the bridge structure, spectral analysis is conducted on generalized forces corresponding to the three modes. The spectral results are plotted against frequency in Figure 4.12a, b, and c for the 1st, 2 nd, and 11th mode, respectively. Figure 4.12 shows that the traditional earthquake forces corresponding to each mode are broadband random processes. Comparatively, coupled earthquake forces mainly have low vibrating frequencies below 0.5 Hz due to the low frequency properties of earthquake ground motion displacements.

Since wheel axles have contact with the bridge girder through the lower springs and dampers, the vibrating modes that correspond to the vibration of wheel axles are more related to bridge-vehicle interactions. Table 2 shows that through the eigenvalue analysis, the fundamental vertical vibrating frequencies for the heavy truck model are 0.89 Hz, 0.89 Hz and 1.01 Hz for the 1st, 2 nd, and 3 rd, wheel axles, respectively. The fundamental lateral vibrating frequencies for the heavy truck model are 0.98 Hz, 0.98 Hz, and 0.55 Hz for the 1st, 2 nd, and 3rd wheel axles, respectively. The fundamental vertical and lateral vibrating frequencies for both wheel axles of the light truck model are 1.11 Hz and 1.20 Hz, respectively. The fundamental vertical and lateral vibrating frequencies for both wheel axles of the light car model are 1.14 Hz and 0.83 Hz, respectively. Because the bridge-traffic interactions are influenced by a number of vehicles for each of the three types of vehicles, this can explain the small peaks of spectral magnitudes for the coupled earthquake force between 0.5 Hz and 1.2 Hz.

The bridge-traffic interaction force has larger spectral magnitudes when coupled with earthquake than when earthquake is not coupled. This is consistent with the observation in the bridge-traffic interaction forces in the time domain. Peaks are found at around 0.42 Hz and 1.20 Hz in the spectral magnitude of bridge-traffic interaction forces with or without coupling with earthquake, which are corresponding to the fundamental vertical and torsional modes of the bridge, respectively. It is inferred in Figure 4.12 that the coupling and interaction forces in the bridge-traffic system under seismic excitations have notable frequency components close to the fundamental frequencies of the bridge and vehicles.

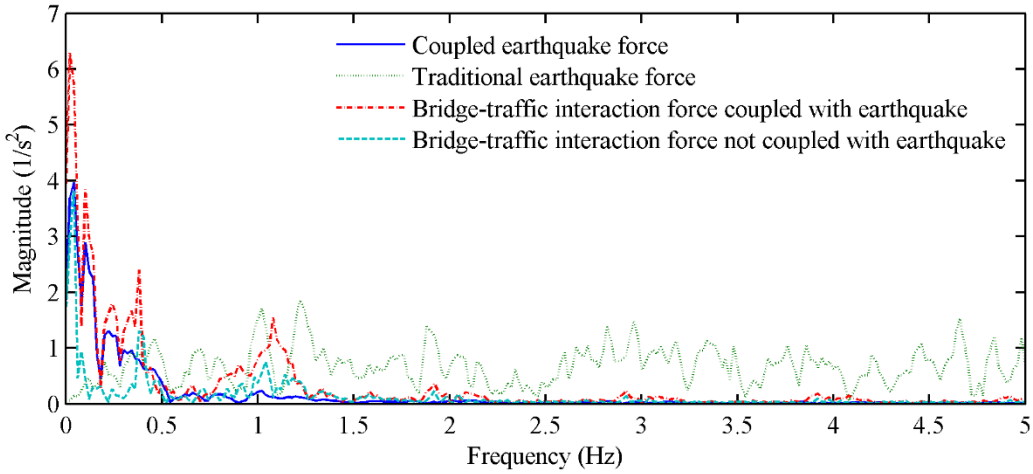

(a) The 1st mode

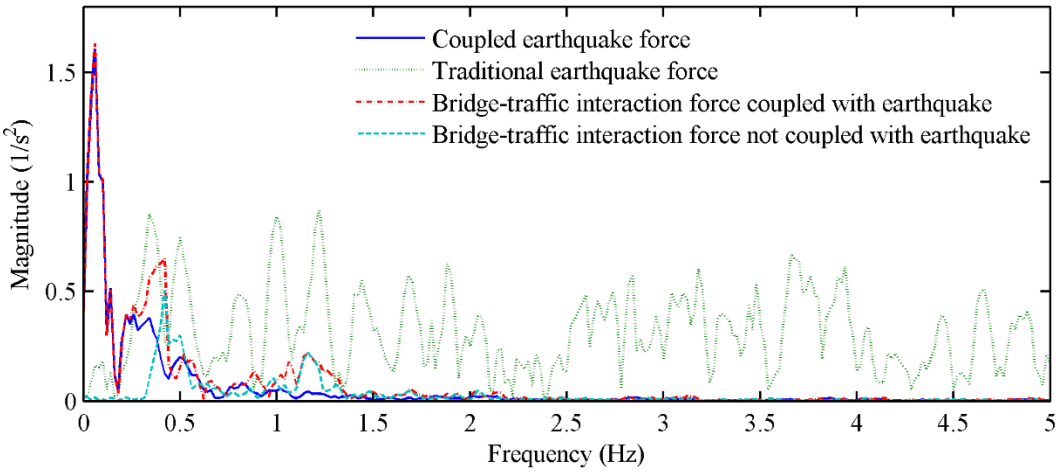

(b) The 2nd mode

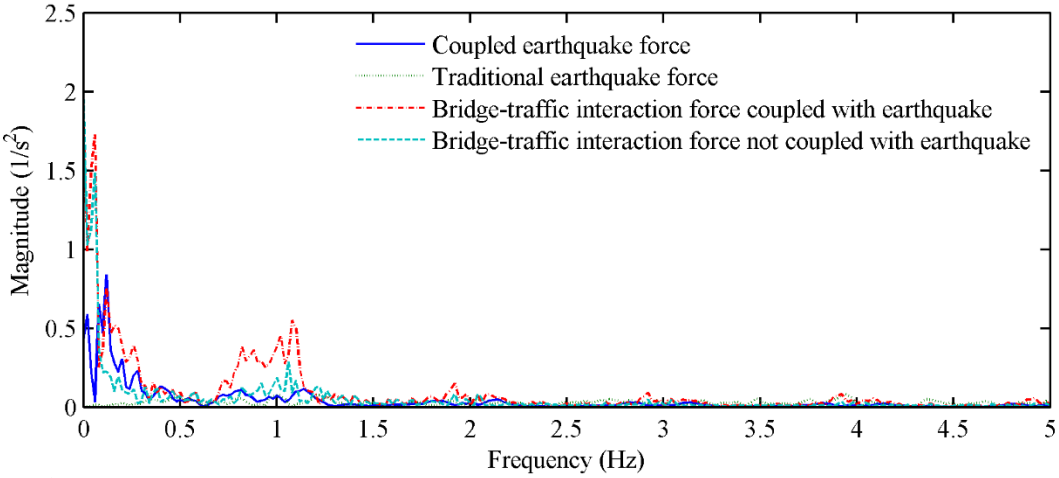

(c) The 11th mode

Figure 4.5 Spectra of generalized forces on the bridge structure corresponding to the fundamental modes

4.5.2 Vehicle Response

The methodology proposed in this study deals with the coupled bridge-traffic system under seismic excitations. In addition to the bridge response, detailed vehicle response considering various sources of coupling effects can be obtained. Unlike the bridge response obtained from the summation of dynamic response and pseudo-static response, the vehicle response is directly obtained from the coupled dynamic analysis in which the earthquake forces are coupled with the bridge-traffic interactions. For moving vehicles in the coupled bridge-traffic system subjected to earthquakes, the sources of excitations include coupled earthquake force and bridge-vehicle interaction force on the vehicle. The bridge-vehicle interaction force on the moving vehicle is obtained from bridge-wheel contact force due to the road surface roughness and coupling effects with the bridge structure. After the vector of generalized coordinate is obtained in each time step from Eq. (30), the bridge-traffic interaction force $F_i^{v\_b}$ on the i^{th} moving vehicle in the traffic flow can be expressed in the following equation:

$$\mathbf{F}_i^{v\_b} = \mathbf{F}_{v_i}^{r} - \sum_{j=1}^{m} \mathbf{K}_{v_i,b} \boldsymbol{\varphi}_j \boldsymbol{\xi}_j - \sum_{j=1}^{m} \mathbf{C}_{v_i,b} \boldsymbol{\varphi}_j \dot{\boldsymbol{\xi}}_j \quad \text{(Eq. 33)}$$

The representative vehicle is selected as a light truck that moves through the bridge and longitudinal location of the light truck with respect to time while it is moving on the bridge as shown in Figure 4.13.

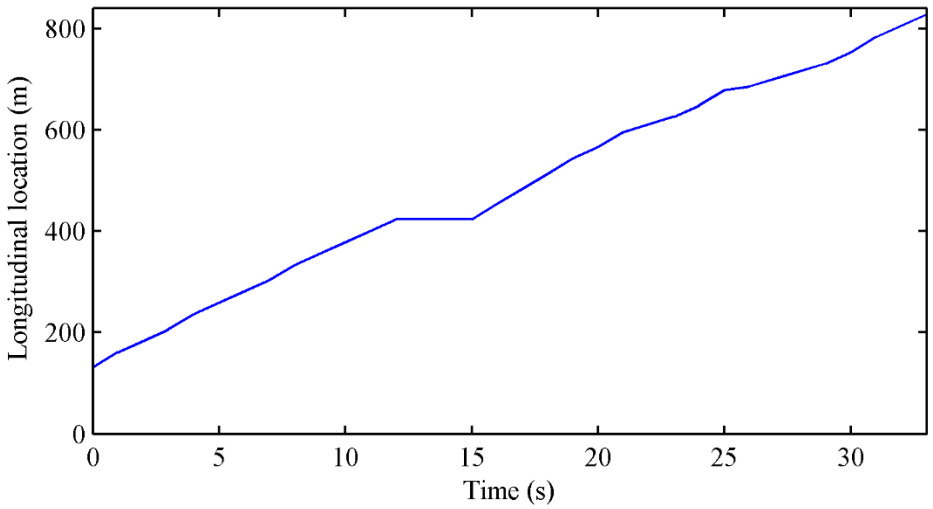

Figure 4.6 Longitudinal location of the representative vehicle on the bridge

Figure 4.13 shows that the vehicle leaves the bridge at around 33.5 s and reaches the bridge middle location of the main span at around 15 s. When the vehicle moves through the bridge, it undergoes acceleration, deceleration, and braking following certain traffic rules. The driving speed of the vehicle is mostly between 22.5 and 30 m/s in a traffic flow with a moderate traffic density. The coupled earthquake force and the bridge-vehicle interaction force on the representative vehicle are obtained and compared. In addition, the bridge-vehicle interaction force of the representative vehicle is obtained and compared when the coupled earthquake force is not considered, and only traditional earthquake force is applied on the bridge structure.

The vertical and lateral contact forces at the left side of the 1st wheel set are obtained for the representative vehicle and shown in Figure 4.14a and b, respectively. The vehicle displacement response is measured from the equilibrium position under vehicle gravity. The vehicle gravity force is not included in the expression of the vehicle vertical contact force in Eq. (33). The coupled earthquake force on the

vehicle may induce an increase on the bridge-vehicle interaction force of the vehicle wheel axle, which is close to the value of the coupled earthquake force itself at certain time instants.

The bridge-vehicle interaction force coupled with earthquake is close to the coupled earthquake force when little bridge-vehicle interaction force is present without coupling with earthquake (Figure 4.14a-b). The coupling effects between the bridge-traffic system and earthquake excitations not only introduce the earthquake force on the vehicle but also significantly change the interaction effects between the vehicle and the bridge. The bridge-vehicle interaction effects on the vehicle become larger when coupled with earthquake forces. In addition, the pseudo-static response of the bridge plays a more important role on the bridge-vehicle interaction effects on the vehicle. Coupled earthquake force on the vehicle tends to be significantly influenced by the pseudo-static response of the bridge in the same motion directions. This is consistent with the formulation of coupled earthquake force on vehicles consisting of bridge-vehicle coupling matrices and pseudo-static response of the bridge.

Figure 4.14a and b show that a peak value of the coupled earthquake force and bridge-vehicle interaction force coupled with earthquake occurs at around 7.0 s due to a peak in the pseudo-static response of the bridge in the vertical and lateral directions, respectively. When the bridge-vehicle interaction force is over the gravity force at the wheel, the vehicle wheel will be separated from the bridge deck. Vehicle gravity at the wheel for the representative light truck is 4.93×10^4 N, which is only a little below the largest upward interaction force, i.e., 5.08×10^4 N as shown in Figure 4.14a. This indicates that vertical separation is not significant even at most unfavorable time instants and the point contact assumption will not cause significant discrepancy from the realistic situation. The lateral contact force can be used to determine if the vehicle will have side-slip at the wheel. When the lateral contact force at a wheel is over the static friction force at the both sides of the wheel, side-slip may occur. Detailed information on the vehicle safety assessment regarding lift-up and side-slip can be found in the Ref (Zhou and Chen 2015b).

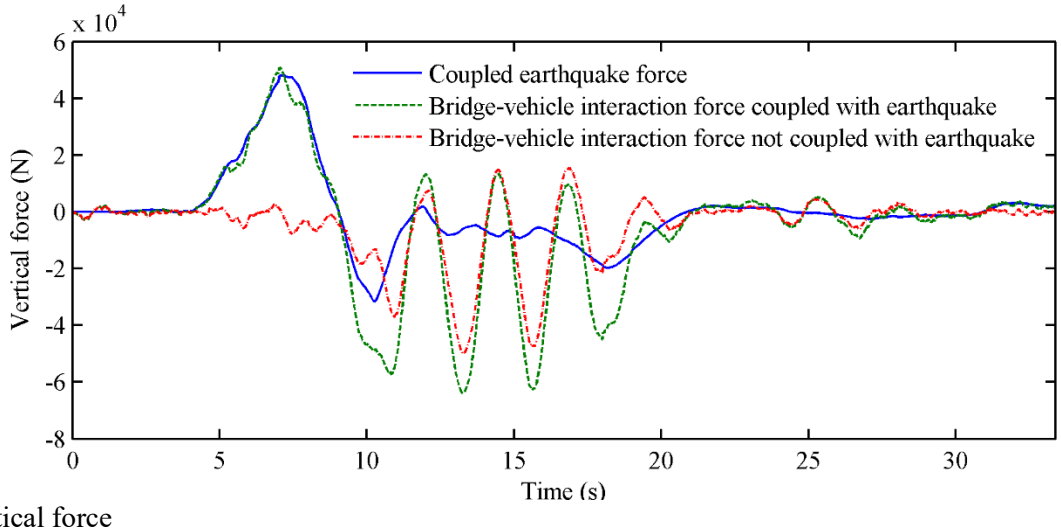

(a) Vertical force

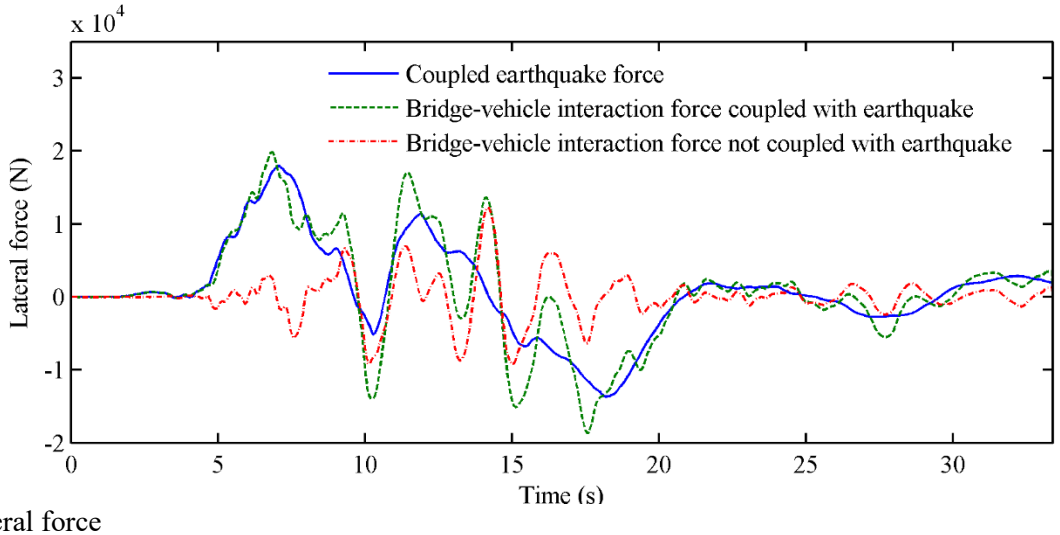

(b) Lateral force

Figure 4.7 The force at the left side of the 1st wheel set of the representative vehicle

The vertical and lateral displacement time histories on the left side of the 1st wheel set are given for the representative light truck in Figure 4.15a and b, respectively. It can be seen that the coupling effects between the earthquake excitations and the bridge-traffic system significantly affect the vehicle response. Larger pseudo-static response on the bridge from earthquake excitations will induce larger dynamic effects on the vehicle in vertical and lateral directions. The bridge-vehicle interaction effects on the vehicle are larger when they are coupled with earthquake. By considering the coupled earthquake force and the bridge-vehicle interaction force coupled with earthquake, the vehicle has a larger extreme response and is therefore at higher risk of exceeding vehicle safety criteria. It again highlights that incorporating coupling effects between the earthquake excitations and the bridge-traffic system is important in predicting the vehicle performance and assessing vehicle safety risk on the bridge during an earthquake event.

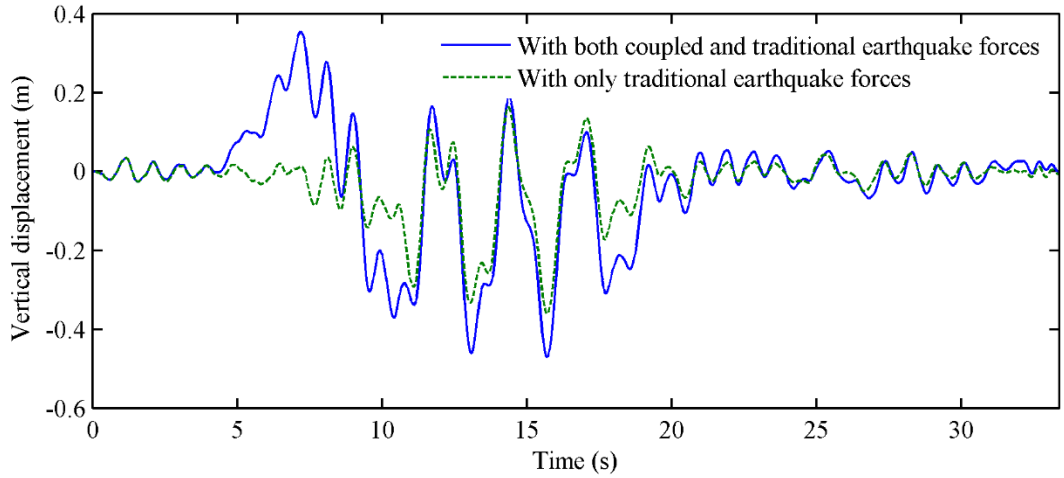

(a) Vertical displacement

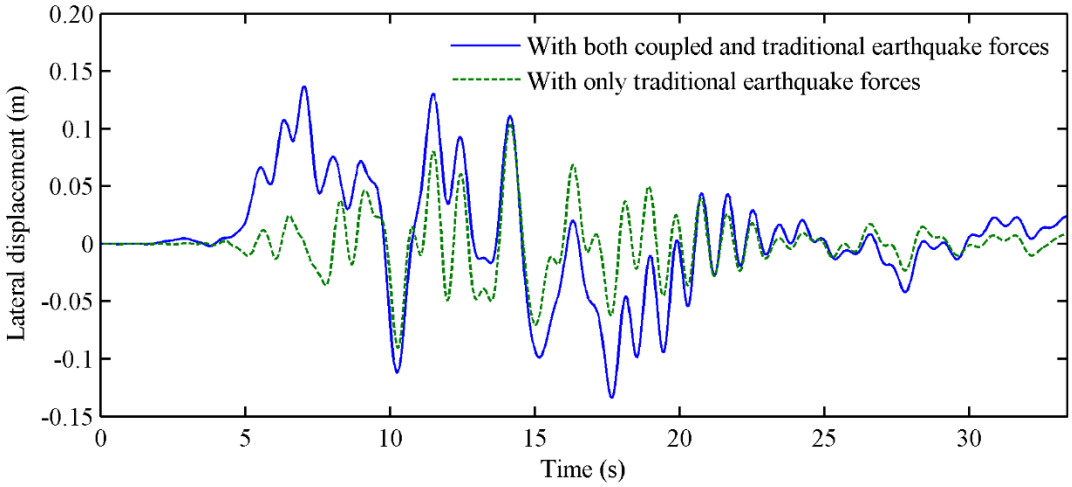

(b) Lateral displacement

Figure 4.8 Comparison of the vehicle dynamic responses with or without coupled earthquake forces

4. CONCLUSION

A full-response prediction framework of the coupled bridge-traffic interaction analysis under non-uniform multi-support seismic excitations was presented based on the acceleration seismic loading method. Different from most existing methodologies for bridge seismic analysis, the proposed new methodology considers the comprehensive coupling effects involved not only between the bridge and vehicles in the traffic flow, but also between the bridge-traffic interacting system and earthquake excitations. In the new methodology, the coupling effects between the bridge-traffic system and earthquake excitations are taken into account by deriving and applying the total equivalent earthquake force on the bridge and vehicles. The total equivalent earthquake force on the bridge is composed of two components, which are traditional earthquake force and coupled earthquake force related to bridge-traffic interactions. Different from the bridge, only coupled earthquake force acts on the vehicles. By taking into account total equivalent earthquake forces on the bridge and vehicles, the complex coupling effects of the bridge-traffic system under seismic excitations can be comprehensively captured and the full seismic responses of the bridge-traffic system can be predicted. In addition, the proposed approach was developed based on seismic acceleration record, which avoids the intrinsic errors existing in the seismic loading method using only earthquake displacements.

The proposed methodology was demonstrated through a prototype long-span cable-stayed bridge and traffic system under spatially varying earthquake excitations. The influences of the moving traffic on the bridge performance and the influences of coupled earthquake force on the bridge and vehicle performance were numerically investigated. The earthquake excitations were generated from a set of typical far-field earthquake record. Conclusions from the numerical studies generally applied to the scenarios subjected to most far-field earthquake ground motions without significant low frequency components below 0.2 Hz. Near-fault earthquakes may have major frequency components below 0.2 Hz, which may pose significant influence on the transient response of long-span bridges. With the scope limit, the coupling behavior of the bridge-traffic system under near-fault earthquake ground motions deserves further investigations. Major findings through the numerical examples are summarized as follows:

- The total bridge response consists of pseudo-static and dynamic response components. The dynamic response components tend to have dominant frequencies close to the fundamental vibration frequencies of the bridge structure, while the pseudo-static response components have much lower frequencies than natural frequencies of the bridge structure.

- The dynamic response components are dominant in the total bridge responses in vertical and rotational directions. In contrast, pseudo-static response is dominant in the total bridge response in the lateral and longitudinal directions.

- Excitations of earthquake and traffic typically cause larger dynamic response on the bridge compared with the response under only earthquake or traffic excitation. Significant nonlinearities were involved in the interaction effects in the coupled bridge-traffic system under seismic excitations.

- The occurrence of earthquake significantly alters the interaction nature between the bridge and moving traffic. Bridge-traffic interaction forces on the bridge become larger when coupled with earthquake ground motions. Coupling effects between the earthquake forces and the bridge-traffic interaction system are stronger in the vertical and torsional directions than those in the lateral direction. The bridge-traffic interaction force coupled with earthquake loads tends to have an opposite phase to the coupled earthquake force on the bridge.

- Coupled earthquake forces on the bridge and vehicles are significantly related to the pseudo-static response of the bridge in the same motion directions. Significant coupling effects between the bridge-traffic system and the earthquake excitations were observed at time instants with larger pseudo-static response of the bridge.

- Incorporation of the coupled earthquake force caused larger extreme responses of the bridge than those only considering traditional earthquake forces, especially in the vertical, lateral and torsional directions. Weights of the traditional earthquake force, coupled earthquake force, and bridge-traffic interaction force out of the total force are found to vary for different motion directions: the traditional earthquake force component is dominant in the total force applied on the bridge for translational modes. The bridge-traffic interaction force coupled with earthquake force becomes dominant for torsional modes.

- The bridge-vehicle interaction effects on the vehicles are larger when coupled with earthquake. By considering the coupled earthquake force on the vehicles, the vehicles exhibit larger extreme response and higher risks of exceeding safety thresholds.

This study assumes that the vehicle wheels and bridge have point contact without separation in the entire simulation process. It was a necessary approximation to simplify the complicated problem of considering the interaction effects in the bridge-traffic system under earthquake. Further studies are required to realistically simulate the contact and separation between the bridge and vehicle wheels in a single simulation process, which still presents a mathematical challenge in the current state of the art. Simulation results from the present study were obtained from the mode superposition approach based on linear dynamic analysis. However, the formulation proposed in this study can be readily extended to nonlinear dynamic analysis in the future if nonlinear finite element approach is adopted with appropriate modeling of geometric and material nonlinearities.

REFERENCES

ASCE (2010). "Minimum Design Loads for Buildings and Other Structures", ASCE/SEI 7-10, American Society of Civil Engineers, Reston, Virginia.

Chen, S. R. and Cai, C. S. (2004). "Accident assessment of vehicles on long-span bridges in windy environments", *Journal of Wind Engineering and Industrial Aerodynamics*, 92 (2004), 991-1024.

Chen, S. R. and Wu, J. (2010). "Dynamic performance simulation of long-span bridge under combined loads of stochastic traffic and wind", *Journal of Bridge Engineering*, ASCE, 15(3), 219-230.

Chen, S. R. and Wu, J. (2011). "Modeling stochastic live load for long-span bridge based on microscopic traffic flow simulation", *Computers & Structures*, 89 (9-10), 813-824.

Deodatis, G. (1996). "Non-stationary stochastic vector processes: seismic ground motion applications", *Probabilistic Engineering Mechanics*, 11 (1996), 149-168.

Du, X. T., Xu, Y. L. and Xia, H. (2012), "Dynamic Interaction of Bridge–train System under Non-uniform Seismic Ground Motion," *Earthquake Engineering and Structural Dynamics*, **41**(1), 139–157.

Léger, P., Idé, I. M. and Paultre, P. (1990). "Multiple-support seismic analysis of large structures", *Computers & Structures*, 36 (6), 1153-1158.

Li, Y. L., Chen, N., Zhao, K. and Liao, H. L. (2012). "Seismic response analysis of road vehicle-bridge system for continuous rigid frame bridges with high piers", *Earthquake Engineering and Engineering Vibration*, 11 (2012), 593-602.

Liu, M. F., Chang, T. P. and Zeng, D. Y. (2011). "The interactive vibration behavior in a suspension bridge system under moving vehicle loads and vertical seismic excitations", *Applied Mathematical Modeling*, 35, 398-411.

MATLAB (Computing Language). MathWorks, Natick, MA.

SAP2000 (V15) (Computer software). Computers and Structures, Berkeley, CA.

Zeng, Q. and Dimitrakopoulos, E. G. (2016). "Seismic response analysis of an interacting curved bridge–train system under frequent earthquakes", *Earthquake Engineering and Structural Dynamics*, 45, 1129–1148.

Zhou, Y. and Chen, S. (2015a). "Dynamic simulation of long-span bridge-traffic system subjected to combined service and extreme loads", *Journal of Structural Engineering*, ASCE, 141 (9), 04014215, 1-18.

Zhou, Y. and Chen, S. (2015b). "Fully coupled driving safety analysis of moving traffic on long-span bridge subjected to crosswind", *Journal of Wind Engineering and Industrial Aerodynamics*, 143 (2015), 1-18.